The *Gaia* view of the Cepheus flare

Máté Szilágyi[1,2][*], Mária Kun[1], Péter Ábrahám[1,3]

[1]*Konkoly Observatory, Research Centre for Astronomy and Earth Sciences, Eötvös Loránd Research Network (ELKH),*
H-1121 Budapest, Konkoly Thege Miklós út 15–17, Hungary
[2]*Department of Astronomy, Eötvös Loránd University, H-1117 Budapest, Pázmány Péter sétány 1/A, Hungary*
[3]*ELTE Eötvös Loránd University, Institute of Physics, Pázmány Péter sétány 1/A, 1117 Budapest, Hungary*

ABSTRACT

We present a new census of candidate pre-main-sequence stars in the Cepheus flare star-forming region, based on *Gaia* EDR3 parallaxes, proper motions, and colour–magnitude diagrams. We identified new candidate members of the previously known young stellar groups associated with NGC 7023, L1177, L1217/L1219, L1228, L1235, and L1251. We studied the 3D structure of the star-forming complex and the distribution of tangential velocities of the young stars. The young stellar groups are located between 330 and 368 pc from the Sun, divide into three kinematic subgroups, and have ages between 1–5 million years. The results confirm the scenario of propagating star formation, suggested by previous studies. In addition to the bulk pre-main-sequence star population between 330 and 370 pc, there is a scattered and more evolved pre-main-sequence population around 150–180 pc. We found new candidate members of the nearby Cepheus Association, and identified a new moving group of 46, 15–20 million years old pre-main-sequence stars located at a distance of 178 pc, around the A0-type star HD 190833. A few pre-main-sequence stars are located at 800–900 pc, indicative of star-forming regions associated with the Galactic local arm above the Galactic latitude of +10°.

Key words: stars: pre-main-sequence – stars: formation – ISM: clouds – ISM: individual objects : Cepheus flare

1 INTRODUCTION

It was noticed by Hubble in 1934 that the opaque belt of the Galactic plane extends to latitudes as high as +20° in the Cepheus, between the Galactic longitudes 93° and 133°. Observations of the atomic and molecular interstellar matter (Heiles 1967; Grenier et al. 1989, respectively) have shown that the obscuring dust belong to two giant interstellar clouds, containing a total mass of some 1.3×10^5 M$_\odot$, and separated from each other in radial velocity. The high-velocity cloud in the $100° < l < 140°$, $+10° < b < +17°$ region and in the $-20\,\mathrm{km\,s^{-1}} < v_{\mathrm{LSR}} < -8\,\mathrm{km\,s^{-1}}$ interval is a high-latitude extension of the Local arm of the Galaxy around 800–900 pc. The low-velocity cloud at $100° < l < 115°$, $+10° < b < +20°$, and in the radial velocity interval $-8\,\mathrm{km\,s^{-1}} < v_{\mathrm{LSR}} < +8\,\mathrm{km\,s^{-1}}$ is a nearby giant molecular complex around a distance of 300 pc, one of the nearest star-forming regions of the northern sky. On the high-longitude side it is bordered by a region free of interstellar matter and radiating in soft X-rays, suggesting a hot bubble, created by a supernova (Grenier et al. 1989). The presence of an expanding shell, named *Cepheus Flare Shell, CFS*, centred on the hot bubble, was identified in the distribution of the neutral hydrogen by Olano, Meschin & Niemela (2006). The CFS might have been created by the winds and subsequent explosion of a high-mass star some 5 million years ago. The giant radio continuum structure *Loop III*, identified by Berkhuijsen (1973) and discernible also in the *WMAP* K-band polarization map (Page et al. 2007) is nearly concentric with the CFS.

The molecular gas of the region was mapped in the ^{13}CO line by Yonekura et al. (1997). The clouds are distributed over a wide range of radial velocities. Several authors argue that this may reflect multiple supernova events in the past (Grenier et al. 1989; Bally & Reipurth 2001; Olano et al. 2006), which might have affected the star formation in this region.

Low-mass young stellar objects (YSOs) of the Cepheus flare are clustered on a few molecular clouds, scattered over the whole surface of the complex (Kun 1998; Kun, Kiss & Balog 2008). Ongoing star formation can be observed in the L1148/L1158 complex, L1172/L1174 (associated with NGC 7023), L1177 (CB 230), L1219, L1228, L1251, L1262 (CB 244) (see Froebrich 2005; Connelley et al. 2008; Kirk et al. 2009, and references therein). A less studied star-forming cloud is L1235, associated with a few optically visible low-mass pre-main-sequence (PMS) stars (Kun et al. 2009) and submillimeter sources (Di Francesco et al. 2008). The small dark cloud Lynds 1221, located near the low-latitude boundary of the region is associated with only deeply embedded young stellar objects (YSOs) (Young et al. 2009), therefore its distance is uncertain. The nearby *Cepheus association* of 20–30 Myr old PMS stars, located at 157 ± 10 pc

[*] E-mail: szilagyi.mate@csfk.org

([Klutsch et al. 2020](#)) is projected at the high Galactic longitude side the Cepheus flare. The very active low- and intermediate-mass star-forming region NGC 7129, located at the low-latitude boundary of the region at a distance of 880 pc ([Reid et al. 2014](#)), is probably associated with the *Cepheus Bubble*, blown by the hot, high-mass stars of the Cepheus OB2 association ([Kun et al. 1987](#); [Ábrahám et al. 2000](#)).

Lists of spectroscopically confirmed PMS stars in the Cepheus flare region were presented by [Kun et al. (2009)](#). [Kirk et al. (2009)](#) published results of the *Spitzer* survey of the most prominent star forming clouds of the Cepheus flare. Most of the stars in both lists are disc-bearing young stars (Class II YSOs, or classical T Tauri stars, CTTS, [Greene et al. 1994](#)). Discless PMS stars (Class III YSOs or weak-line T Tauri stars, WTTS), distributed over the surface of the Cepheus flare, were identified by [Tachihara et al. (2005)](#).

The cloud complex extends over some 15 degrees in Galactic longitude, corresponding to some 90 pc at the mean distance of 350 pc ([Dzib et al. 2018](#)). This size suggests a significant depth of the cloud complex along the line of sight. The precise positions, parallaxes, proper motions, and photometry of the optically visible young stars, measured by the *Gaia* mission ([Gaia Collaboration et al. 2016](#)), opened the door to studying of the spatial structure and internal motions of star-forming regions.

The overall properties of the Cepheus flare, based on *Gaia* DR2 ([Gaia Collaboration et al. 2018](#)) data of 47 pre-main-sequence (PMS) stars were investigated by [Dzib et al. (2018)](#) during the study of the *Gaia* view of the Gould Belt system of the nearest star-forming regions. They found that the average distance of the known young stars of the Cepheus flare, included in the *Gaia* DR2, was 360 ± 32 pc. They also found that the proper motion dispersions of the studied stars were large compared to those of other regions.

[Green et al. (2019)](#) presented three-dimensional maps of Galactic dust reddening, based on *Gaia* parallaxes and stellar photometry from Pan-STARRS 1 and 2MASS. The maps suggest that the clouds of the Cepheus flare are located between 320 and 370 pc, and toward a few lines of sight there is a more distant layer of dark clouds between 850–1000 pc.

[Zari et al. (2018)](#) selected pre-main-sequence stars and young upper main sequence stars in the solar neighbourhood from the *Gaia* DR2 based on a combination of astrometric and photometric criteria. Their catalogue of pre-main-sequence stars contains 826 stars in the $100° \leq l \leq 124°$, $8° \leq b \leq 24°$ area and closer than 500 pc to the Sun. This sample is biassed against the youngest members of the PMS population, whose photometric properties are affected by the circumstellar disc and envelope.

The recently released *Gaia* EDR3 ([Gaia Collaboration et al. 2021](#)) represents a significant improvement with respect to *Gaia* DR2 in terms of astrometric and photometric precision, accuracy, and homogeneity. In this paper we present a view of the Cepheus flare based on *Gaia* EDR3 data. We examine the star-forming molecular clouds of the Cepheus flare one by one. We derive mean distances and tangential velocities of the young stellar groups associated with individual clouds, and identify new candidate members. To characterize the new candidate young stars we examine their G vs. $(G-G_{\rm RP})$ colour–magnitude diagram, *2MASS* and *WISE* colour–colour diagrams, and estimate mean ages using the

PARSEC ([Bressan et al. 2012](#)) isochrones for stars more massive than 1.4 M$_\odot$ and CIFIST ([Baraffe et al. 2015](#)) for the stars below this mass. We present our initial sample of young stars in Sect. 2. Our search for new members is described in Sect. 3, and the results are presented and discussed in Sects. 4 and 5. We summarize the main results in Sect. 6.

2 DISTANCES AND TANGENTIAL VELOCITIES OF INDIVIDUAL YOUNG STELLAR GROUPS

In order to determine the mean distances and the range of proper motions of young stellar objects associated with individual molecular clouds we compiled an initial list of *Gaia* EDR3 counterparts of known, optically visible YSOs in the $100° < l < 125°$, $+8° < b < +22°$ region, consisting of spectroscopically identified YSOs published in [Kun et al. (2009)](#), *Spitzer* sources, identified as flat-SED and Class II YSOs by [Kirk et al. (2009)](#), spectroscopically identified weak-line T Tauri stars from [Tachihara et al. (2005)](#), and spectroscopically identified WTTS members of the *Cepheus Association* from [Klutsch et al. (2020)](#).

We searched *Gaia* EDR3 counterparts of these stars within 1 arcsec. Nine of the 77 pre-main-sequence stars listed in [Kun et al. (2009)](#) are associated with NGC 7129 at a distance of 880 pc, and three further ones (2MASS J21225426+6921344, [KBK2009b] Em* 119 S, and TYC 4608-2063-1) are located far beyond the molecular complex. Based on the angular separations and position angles listed in [Kun et al. (2009)](#) we could identify both components of the visual binary T Tauri stars Cl* NGC 7023 RS 5, LkHα 428, OSHA 48, OSHA 50, and [K98c] EM*119. Sixty-six infrared sources, classified as YSOs in [Kirk et al. (2009)](#), and missing from the above list, coincide with *Gaia* EDR3 sources within 1 arcsec. Sixteen weak-line T Tauri stars, resulted from spectroscopic observations of *ROSAT* X-ray sources in [Tachihara et al. (2005)](#), have *Gaia* EDR3 counterparts within 1 arcsec. These stars are projected outside of the molecular clouds and are located at various distances. Twenty-nine pre-main-sequence stars were identified by [Klutsch et al. (2020)](#) as members of the nearby *Cepheus Association*. Each of them have *Gaia* EDR3 counterpart, and seven of them coincide with weak-line T Tauri stars identified by [Tachihara et al. (2005)](#). We used four additional stars from [Faherty et al. (2018)](#) which appear in [Klutsch et al. (2020)](#) as a *Cepheus Association* bona-field members. After removing the duplicates, our initial list contains 176 known young stars. We supplemented the data in our initial list with distances, derived by [Bailer-Jones et al. (2021)](#) from *Gaia* EDR3 parallaxes, using a prior constructed from a three-dimensional model of our Galaxy, which takes into account the interstellar extinction and *Gaia*'s variable magnitude limit. Using Astropy ([Astropy Collaboration et al. 2013](#)) we transformed the proper motion components into Galactic proper motions, and using the distances the Galactic tangential velocity components were calculated. The initial list of young stars with *Gaia* EDR3 counterparts is shown in Table A1. Their distribution in Galactic coordinates is plotted with red squares in the upper panel of Fig. 1. Green crosses in the same panel show candidate pre-main-sequence stars from [Zari et al. (2018)](#). Symbol colours in the lower panel indicate distance intervals.

Then we defined areas of the sky containing the clouds

and their associated YSOs. To include possible scattered young stellar populations outside of the visible boundaries of the clouds we defined wide tetragons encompassing the clouds. The tetragons are shown in Fig 1. In addition to the known star-forming molecular clouds we defined two large regions containing numerous pre-main-sequence stars and candidates closer than 200 pc (*Cepheus Association* and *HD 190833 Group*, see Section 3.2). We suppose that the candidate pre-main-sequence stars from Zari et al. (2018), projected within our tetragons, are members of the YSO clusters and use them to derive the mean distance and tangential velocity components of the clusters.

We plotted in Fig. 2 the distance histogram of the YSOs listed in Table A1 and candidates from Zari et al. (2018) for each region labeled in Fig. 1, and identified the obviously foreground and background stars of the area. After removing these stars from the lists we calculated the mean parallax and proper motion components of the stars for each region. During this process we used only stars which fulfilled the astrometric criteria as follows: $\varpi/\sigma_\varpi > 10$, $|\mu_\alpha^\star/\sigma_{\mu_\alpha^\star}| > 2$, $|\mu_\delta/\sigma_{\mu_\delta}| > 2$ and RUWE < 1.6, where ϖ and σ_ϖ are the parallax and parallax error, $\mu_\alpha^\star$, μ_δ and $\sigma_{\mu_\alpha^\star}$, σ_{μ_δ} are the proper motion components in ICRS ($\mu_\alpha^\star = \mu_\alpha cos\delta$), and their uncertainties, respectively, and RUWE is the re-normalized unit weight error, described in Lindegren (2018). Table 1 shows the central positions in Galactic coordinates, average parallaxes and proper motions of the YSOs of each cloud. The host molecular clouds, their distances, obtained from the 3D extinction maps of Green et al. (2019), and radial velocities, found in Yonekura et al. (1997) and Clemens & Barvainis (1988) are also listed.

Based on the stars that fulfil our astrometric criteria we defined the distance and tangential velocity ranges of the confirmed and candidate YSOs for each region listed in Table 1. First we calculated the median-absolute-deviation (MAD) of the distances for each region:

$$\mathrm{MAD(d) = median(|d - d_{med}|),} \qquad (1)$$

and adopted the distance range $\mathrm{d_{med} \pm 5\,MAD(d)}$ as the line-of-sight extent of the cluster. We examined the velocity ranges of the stars in these distance intervals and found that they are within $\mathrm{v_{l,med} \pm 5\,MAD(v_l)}$, $\mathrm{v_{b,med} \pm 5\,MAD(v_b)}$ for most of the clouds. An exception is L1228, where we used 3 MAD for the distance and 4 MAD for the velocities. The candidate PMS stars in the catalogue of Zari et al. (2018), projected into the area of L1148/L1158 complex have a variety of motion directions. Apparently they do not constitute a comoving system. Therefore the tangential velocity ranges for this area were defined by the three stars listed in Kun et al. (2009) and Kirk et al. (2009). Table 2 lists the boundaries of the tetragons and minimum and maximum values of the distances and velocities.

We find that the YSOs, clustered on the dark clouds, are located between 300 and 400 pc. A few T Tauri stars of the initial list are situated beyond 500 pc, indicative of distant star-forming regions around 800–1000 pc. Stars with $100\,\mathrm{pc} < d < 200\,\mathrm{pc}$ are found in two large areas in the high-latitude part of the studied region.

3 NEW MEMBERS DEFINED BY DISTANCES AND TANGENTIAL VELOCITIES

3.1 Selection criteria

We search for further members of the star-forming clouds in *Gaia* EDR3 based on the distances and tangential velocities, defined by the stars of our initial sample. First we selected all sources from *Gaia* EDR3 with:

- $100° < l < 125°$,
- $8° < b < 22°$,
- $d < 500\,\mathrm{pc}$,
- $\varpi/\sigma_\varpi > 10$,
- $|\mu_\alpha^\star/\sigma_{\mu_\alpha^\star}| > 2$,
- $|\mu_\delta/\sigma_{\mu_\delta}| > 2$,
- RUWE < 1.6,

where l and b are the galactic longitudes and latitudes, d is the distance (column r_med_geo) from Bailer-Jones et al. (2021). Using Astropy we transformed the proper motion components into Galactic proper motions, and using the distances the Galactic tangential velocity components were calculated.

We selected new candidate cluster members from the filtered *Gaia* EDR3 list using the distance and tangential velocity ranges defined in Sect. 2. No photometric constraint was applied during this process. The selection resulted in 266 new candidate members of the targeted clouds. Figures 7a–12a show the surface distributions and tangential velocities of the cluster stars. Red symbols indicate stars of the initial list, green crosses mark the comoving members from Zari et al. (2018), and blue symbols show the new candidate cluster members. Parallax histograms are plotted in Figs. 7c–12c. The colour–magnitude diagrams in Figs. 7e–12e support the pre-main-sequence nature of the newly identified kinematic cluster members (see Sect. 3.3).

Gaia EDR3 identifiers, coordinates, distances, tangential velocities along Galactic longitude and latitude, and other names of these stars are listed in Table A2. The number of confirmed YSOs with reliable *Gaia* EDR3 data (N), the number of comoving candidate members ($\mathrm{N_{cand}}$), mean parallaxes and tangential velocities of the clusters supplemented with the new candidate members are shown in Table 5.

3.2 Pre-main-sequence stars not associated with molecular clouds

After selecting YSO candidates associated with molecular clouds we analyzed the remaining pre-main-sequence star candidates from the catalogue of Zari et al. (2018). Two large groups of stars at $140-200\,\mathrm{pc}$ to the Sun show up in the lower panel of Fig. 1. One of them at the eastern part of our studied region is projected onto the region devoid of molecular gas, bordering the Cepheus flare. Several publications have already studied comoving stars in this region. Guillout et al. (2010) identified four lithium-rich comoving stars, and Faherty et al. (2018) listed seven stars in this region, three of which are identical with those in Guillout et al. (2010). Klutsch et al. (2020) identified 29 further pre-main-sequence members of this group via high-resolution spectroscopy of X-ray source counterparts, and derived a mean distance of $157\pm10\,\mathrm{pc}$ and age of 10–20 million years. We adopt the name *Cepheus Association* from their work. We note that while the
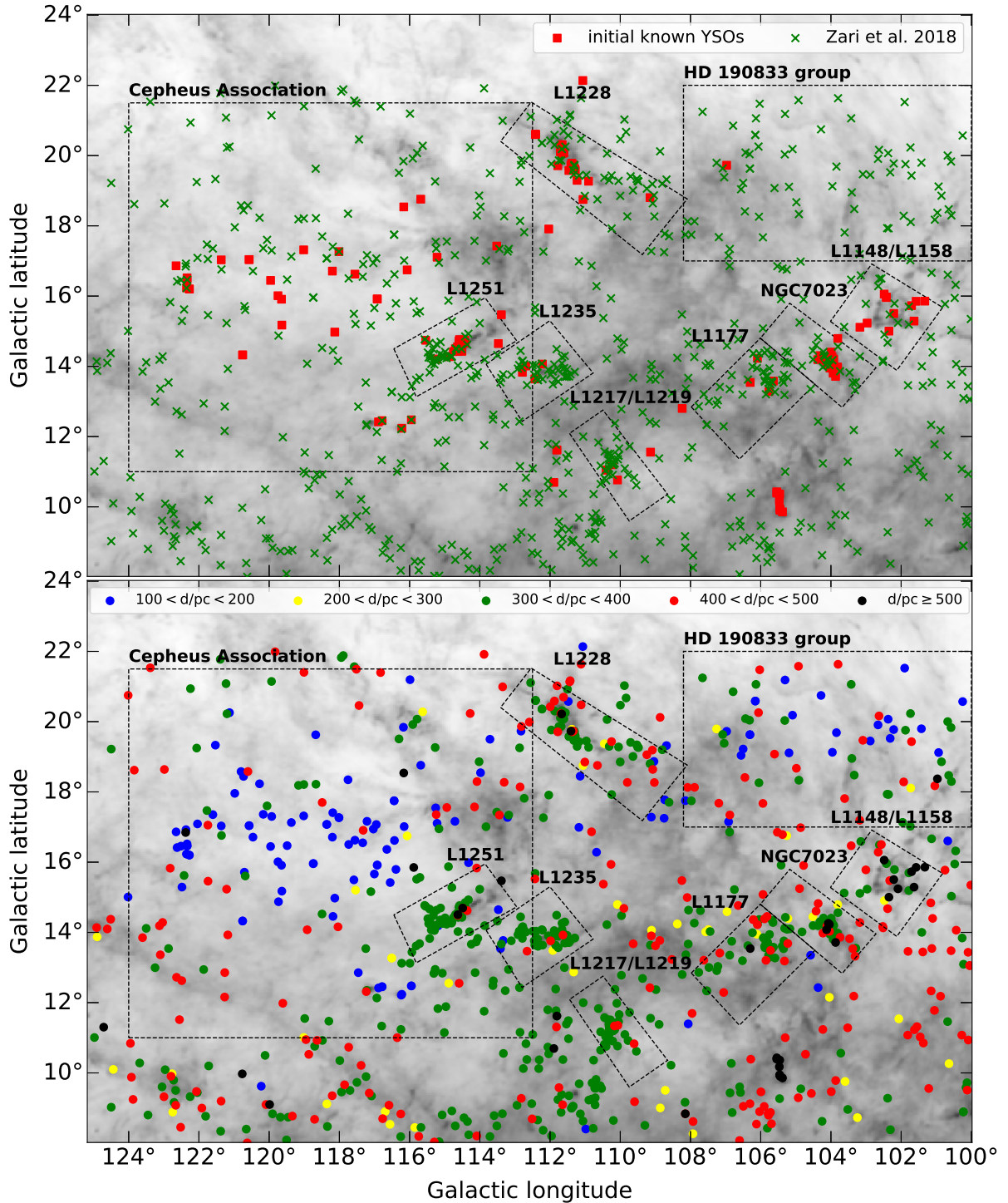
Figure 1. *Top*: Distribution of spectroscopically confirmed young stars and *Spitzer* sources (red squares) from our initial list and candidate pre-main-sequence stars of Zari et al. (2018) (green crosses) in Galactic coordinates, overplotted on the *Planck* 857 GHz map of the region. *Bottom*: Same as the upper panel, but the symbol colours indicate distances.

gas-free region itself is thought to be a supernova bubble, interacting with the molecular clouds of the Cepheus flare, the young stars projected within this area are much closer to the Sun. The other group is located at the northwestern part of the Cepheus flare. We defined two rectangles (see Table 3 for the boundaries) to search for additional group members.

Since these groups stretch over several degrees, the proper motions of stars, having common space motions, may not be identical over the whole area, thus the method described in Section 3.1 cannot be applied. To identify comoving stars within these large areas we followed the method described in Damiani et al. (2019): stars having the same space motion
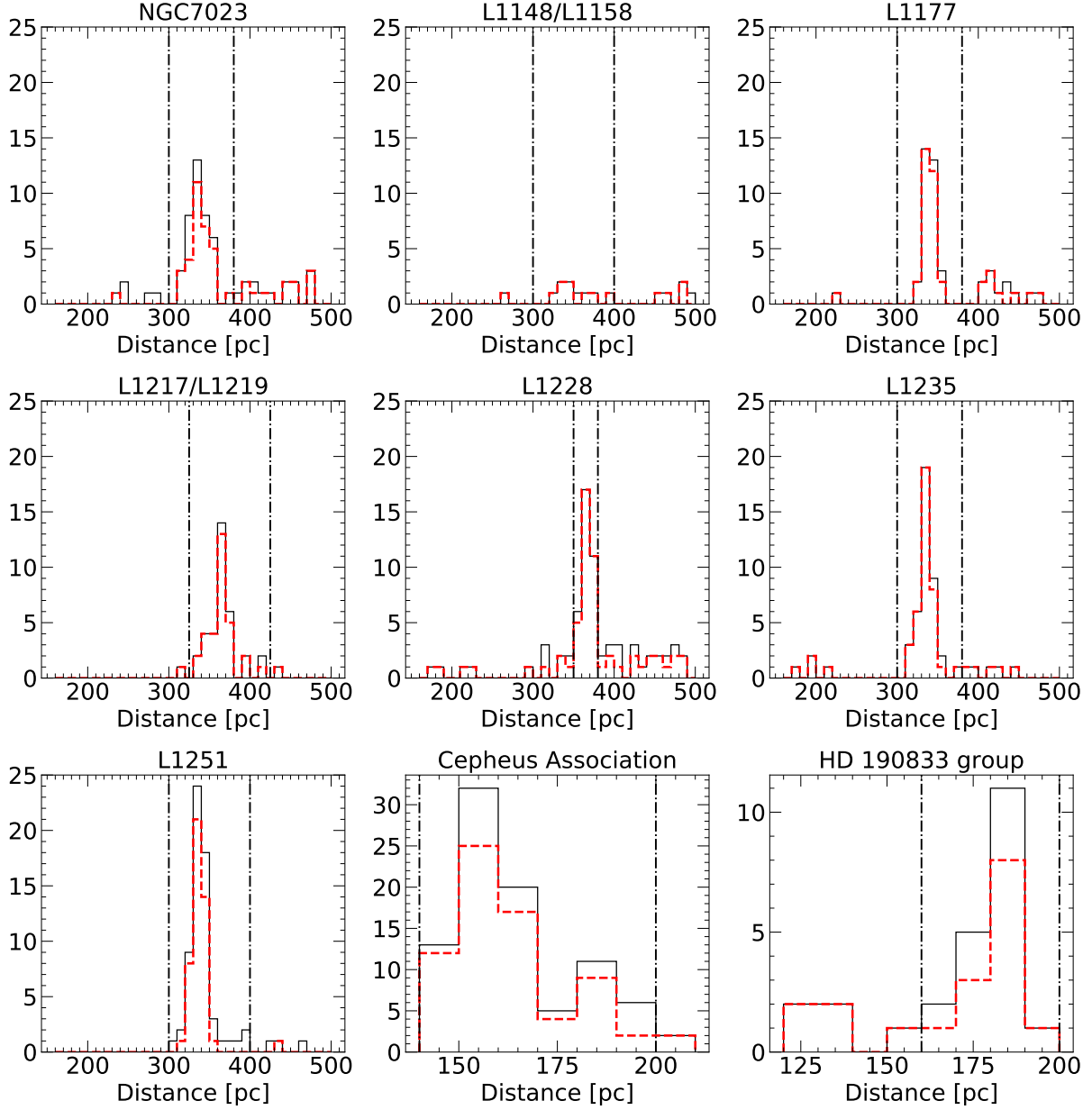
Figure 2. Distance histograms of the YSOs of our initial list supplemented with candidates from Zari et al. (2018). The thin black lines indicate all stars, and the thick red dashed lines show stars with $\varpi/\sigma_\varpi > 10$, $|\mu_\alpha^\star/\sigma_{\mu_\alpha^\star}| > 2$, $|\mu_\delta/\sigma_{\mu_\delta}| > 2$ and RUWE < 1.6. The sources outside the region bounded by vertical dashed-dotted lines are considered fore- or background stars and were disregarded. For plotting purposes we did not plotted stars with distances larger than 500 pc.

should fall along a straight line in the $(tan(l), v_l/cos(l))$ plane, whose slope and intercept provide the space velocity components U and V of the kinematic group, respectively. Figure 3a shows the distribution of the members of the Cepheus Association (red squares, from Klutsch et al. 2020), and the candidate pre-main-sequence stars with 140 pc < d < 200 pc from Zari et al. (2018, green crosses) in the $v_l/cos(l)$ vs. $tan(l)$ plot. The straight line is fitted to all points displayed. The grey band indicates the formal uncertainty of the fitted line. We selected the stars inside the grey bands, and using the U and V velocity components derived from the fitted line calculated their W velocity component (eq. 17 in Damiani et al. 2019). The new candidate members of the kinematic group

were selected using the histograms of W, displayed in Fig. 3b. The derived W velocities are distributed over a narrow range mainly between -10.5 and -9 km s^{-1}, thus we adopted all of them as candidate members.

We used the same method for selecting members from the catalogue of Zari et al. (2018) and *Gaia* EDR3 between 160 and 200 pc in the other area, labeled as *HD 190833 group* after the brightest candidate member. Figure 4a shows *Gaia* sources with $v_l/cos(l)$ between -60 and -40 km s^{-1}, where the candidate YSOs of Zari et al. (2018) are located. The straight line in Fig. 4a is fitted to the sources of Zari et al. (2018) and [TNK2005] 20. Figure 4b shows that the W distribution has two peaks at around -13.5 and -10 km s^{-1},

Table 1. Central positions, mean parallaxes and proper motions of young stellar groups, and distances and radial velocities of their associated molecular clouds

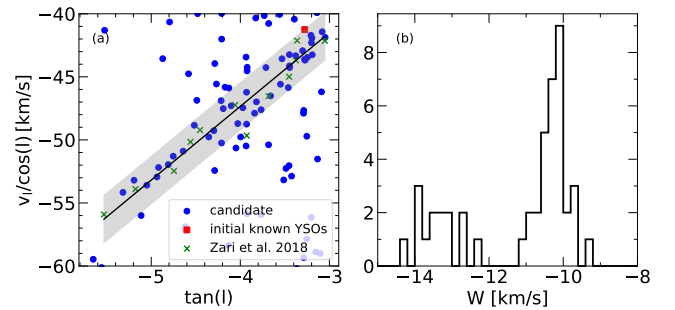| Name | l | b | ϖ | μ_α^* | μ_δ | Molecular Cloud | | |
						Name	Distance*	$v_{\rm LSR}$
	(deg)		(mas)	(mas yr^{-1})			(pc)	(km s^{-1})
L1155	102.60	15.25	2.978	7.971	-1.699	[YDM97] CO 8	341	2.9
L1174	104.06	14.19	2.943	7.480	-1.504	[YDM97] CO 14	341	2.7
L1177	105.17	13.16	2.903	8.041	-1.016	CB 230	300	2.9
L1219	110.59	12.07	2.605	5.055	1.439	[YDM97] CO 57	370	-4.6
L1228	111.67	20.22	2.683	5.148	3.835	[YDM97] CO 66	381	-7.6
L1235	112.24	13.89	2.908	5.400	1.649	[YDM97] CO 69	330	-4.0
L1251	114.51	14.65	2.919	6.828	0.931	[YDM97] CO 79	341	-3.8
L1262	117.20	12.36	6.346	21.647	1.409	[YDM97] CO 101	210	3.9

*Estimated on the 3D extinction map of Green et al. (2019).

Table 2. Boundaries defined for the clouds, minimum and maximum distances and tangential velocities of their known members.

Cloud	RA$_{\rm min}$	RA$_{\rm max}$	Dec$_{\rm min}$	Dec$_{\rm max}$	d$_{\rm min}$	d$_{\rm max}$	v$_{l,\rm min}$	v$_{l,\rm max}$	v$_{b,\rm min}$	v$_{b,\rm max}$
	(deg)				(pc)		(km s^{-1})			
NGC7023	313.75	317.50	67.00	70.00	301.506	372.512	3.246	8.206	-12.759	-8.401
L1148/L1158	307.50	313.00	66.50	68.80	327.065	332.835	4.423	5.622	-12.286	-11.713
L1177	317.50	325.50	68.00	70.00	319.607	358.173	5.989	9.559	-12.159	-9.272
L1217/L1219	331.40	335.00	68.50	71.50	338.535	395.330	6.763	10.036	-5.532	-2.292
L1228	311.25	318.50	74.00	79.00	355.051	380.205	8.580	13.183	-7.716	-0.578
L1235	330.00	338.00	72.50	74.41	317.331	357.335	6.685	10.370	-4.139	-1.653
L1251	334.00	346.00	74.50	76.00	312.153	363.027	6.807	14.518	-6.705	-2.860
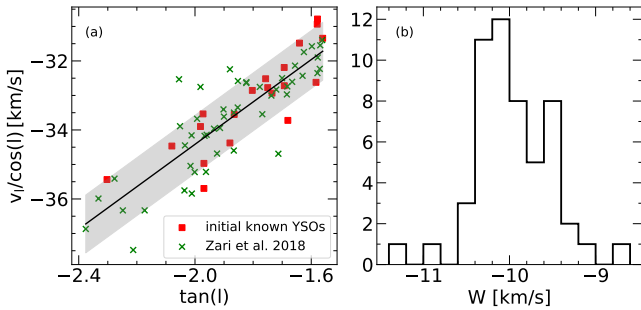
Figure 3. *a*: Distribution of the members and new candidate members of the Cepheus Association in the $(tan(l), v_l/cos(l))$ plane. *b*: Histogram of the W velocities computed for the stars in the shaded area of panel (a).

Figure 4. Same as Fig. 3, but for the HD 190833 moving group.

3.3 Characterising the YSO groups and new candidate members

Minimum spanning trees. We constructed minimum spanning trees (MST) to characterise the size and structure of the identified clusters and aggregates. Figures 7b–14b show the MSTs for each cloud.

Tangential velocities. We calculated velocities compared to the *Local Standard of Rest* (LSR) by subtracting from the tangential velocities the (l,b) components of the Solar peculiar motion, using the U, V, W velocity components of Solar motion determined by Schönrich et al. (2010). Figure 5 shows the distribution of the members of individual groups in the $v_{b,\rm LSR}$ vs. $v_{l,\rm LSR}$ plane. The same distributions are displayed for each group separately in Figs. 7d–14d. The av-

suggesting that the *Gaia* DR3 stars, grouped around the fitted line of Fig. 4a, form two kinematic subgroups, which differ only in the velocity component W, perpendicular to the Galactic plane. We adopt the stars of both subgroups as candidate members of the HD 190833 moving group.

Figure 13a and 14a show the surface distributions and tangential velocities of of the candidate members of these nearby moving groups. The mean space velocity components of the two groups, derived during this process, are listed in Table 3. *Gaia* EDR3 identifiers, coordinates, distances, tangential velocities along Galactic longitude and latitude, and other names of the new candidate group members are listed in Table A2.

Table 3. Boundaries and mean U, V, W velocities derived for the Cepheus Association and HD 190833 group.

	Cepheus Association	HD 190833 group
$l_{\min}$	112°5	100°
$l_{\max}$	124°	108°
$b_{\min}$	11°	17°
$b_{\max}$	21°	22°
U (km s^{-1})	6.1 ± 0.4	5.8 ± 0.5
V (km s^{-1})	-22.1 ± 0.8	-24.0 ± 1.9
W (km s^{-1})	-10.0 ± 0.4	-11.2 ± 1.5

erage velocity components of the whole system of candidate pre-main-sequence stars, corrected for the reflex solar motion, are $v_{l,\mathrm{avg}}^{\mathrm{LSR}} = 8.3 \pm 2.4\,\mathrm{km\,s^{-1}}$ and $v_{b,\mathrm{avg}}^{\mathrm{LSR}} = -6.7 \pm 3.9\,\mathrm{km\,s^{-1}}$.

Colour–magnitude diagrams of the young clusters. To have an insight into the relative ages of the YSO groups, G vs. $(G-G_{\mathrm{RP}})$ colour–magnitude diagrams of confirmed and candidate pre-main-sequence members of individual dark clouds are plotted in Figs. 7e–14e. Isochrones of 1, 10, and 20 million years of the PARSEC (Bressan et al. 2012) models for masses above 1.4 M$_\odot$ and CIFIST (Baraffe et al. 2015) models for masses below 1.4 M$_\odot$ are also plotted.

2MASS colour–colour diagrams. To assess the nature of the newly identified candidate pre-main-sequence stars we supplemented the *Gaia* data with 2MASS (Skrutskie et al. 2006) data. To search for 2MASS counterparts of the stars, we transformed ICRS coordinates from *Gaia*'s J2016 epoch into J2000 epoch. Then we searched for coinciding 2MASS sources within 1 arcsec. Several binary systems in the initial list have separations larger than 1 arcsec, but were identified as single 2MASS sources. In those cases we manually crossmatched the 2MASS with the *Gaia* data. $J-H$ vs. $H-K_{\mathrm{s}}$ colour-colour diagrams of the clusters are shown in Figs. 7f–14f.

WISE colour–colour diagram. Mid-infrared colour indices are helpful in identifying disc-bearing pre-main-sequnce stars. Whereas *Spitzer* observed only a small fraction of the studied area, *WISE* (Wright et al. 2010) data at 3.4, 4.6, 12.0, and 22.0 μm are available for the whole region in the *All-WISE* data base. We found *WISE* counterparts of 313 candidate YSOs within 1 arcsec. To identify infrared-excess stars, we followed the methods described by Koenig & Leisawitz (2014). Of the 313 *WISE* sources, 225 fulfil the quality criteria essential for constructing their $(w1 - w2)$ vs. $(w2 - w3)$ colour-colour diagram, displayed in Fig. 6. Thirty-five of the displayed points lie within the area of the Class II sources, defined by Koenig & Leisawitz (2014). Involving 2MASS data the $(H - K_{\mathrm{s}})$ vs. $(w1 - w2)$ diagram resulted in three further Class II sources, and two candidate transitional discs were identified in the $(w1 - w2)$ vs. $(w3 - w4)$ diagram. The candidate disc-bearing YSOs are listed in Table A3. We encircled these sources with black diamonds in Figs. 7a–14a.

Interstellar extinction towards the YSO groups. We obtained reddening versus distance curves for the nominal *Simbad* positions of the molecular clouds from the 3D maps of Green et al. (2019), except for HD 190833 group, where we used
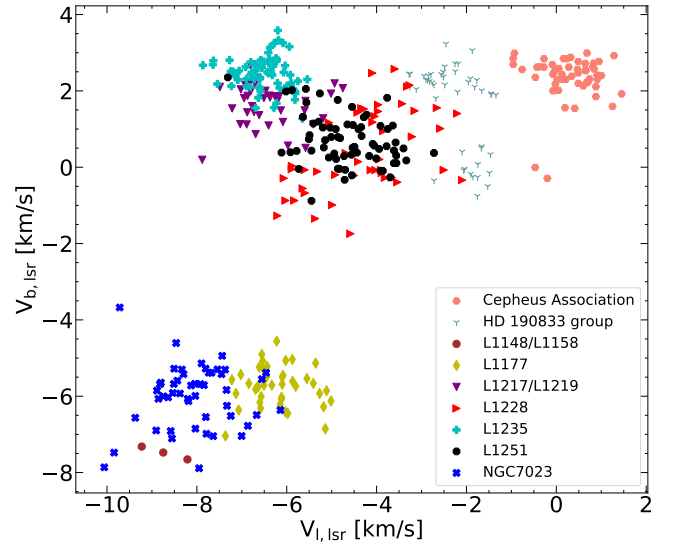

Figure 5. Tangential velocities of the members and candidate members of the subregions of the Cepheus flare as compared to the Local Standard of the Rest.
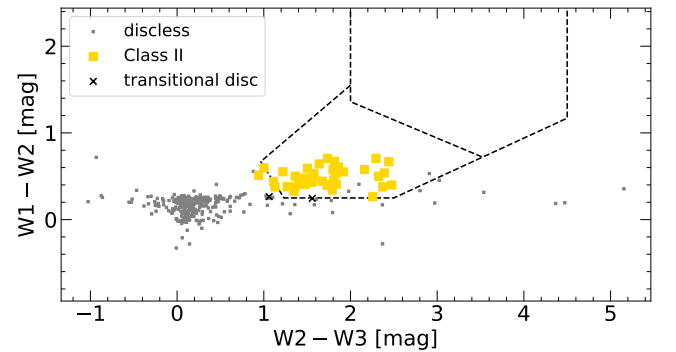

Figure 6. *AllWISE* colour–colour diagram of the newly identified candidate YSOs of the Cepheus flare. Dashed lines border the areas occupied by Class I and Class II YSOs, according to Koenig & Leisawitz (2014).

the central coordinates of the tetragon. We used the Python-implemented `dustmap` package with the best fitted model to download the reddenings and $R_V = 3.1$ to transform them into A_V extinctions (see Figures 7a–14g).

4 RESULTS FOR THE INDIVIDUAL MOLECULAR CLOUDS AND YSO GROUPS

L1148/L1158. Our initial list of YSOs contains 11 objects projected on this cloud complex. Eight of them fulfil our astrometric quality criteria. Only three of the eight – RNO 124, SSTgbs J2048103+6803019, and SSTgbs J2036116+6757093 – have distances compatible with the cloud complex. (The fourth known optically visible YSO of the region, PV Cep has RUWE = 2.4, indicative of uncertain astrometric data.) Five of the 8 sources have distances between 607 and 1080 pc. All of them were detected only by the MIPS instrument of

Spitzer at $24\,\mu$m, and were classified as off-cloud objects by Kirk et al. (2009). They suggest the presence of a star-forming region between these distances. The A_V vs. D diagram in Fig. 7g and the catalogue of Zucker et al. (2020) also indicate the presence of a distant layer of obscuring matter towards some nearby lines of sight.

The 12 candidate PMS stars in Zari et al. (2018), projected onto these clouds, differ in parallax and proper motion from the confirmed YSOs and from each other. The *Planck* 857 GHz map of the L1148/L1158 cloud complex and its associated *Gaia* stars are shown in Fig. 7a, together with the neighbouring NGC 7023.

NGC 7023. This region was recently studied in detail by Saha et al. (2020). They identified 20 new members of the cluster based on *Gaia* DR2 data, and derived a distance of 335 ± 11 pc. Our initial list contain 37 spectroscopically or *Spitzer*-classified YSOs, projected within the tetragon containing the NGC 7023 cluster, 22 of which fulfil our astrometric quality criteria. One of them, SSTgbs J2104156+6742464 is located far beyond the cluster. When defining the tangential velocity ranges, we used 19 stars within the intervals listed in Table 2. These stars are plotted with red symbols in Fig. 7). Based on *Gaia* EDR3 data we identified 31 comoving stars within the defined tetragon (green and blue symbols in Fig. 7). Ten of the 31 are found in the catalogue of Zari et al. (2018). The mean distance of the cluster +/- the standard error of the mean is 341 ± 2 pc. The colour–magnitude diagram (Fig. 7e) suggest moderately reddened low-mass YSOs. Taking into account an average foreground extinction of 1.6 mag (Saha et al. 2020) we estimate an age of some 1 million years. The star below the 20-Myr isochrone of the colour–magnitude diagram in Fig. 7e is Cl*NGC 7023 RS 10, whose spectral energy distribution suggests a Class I YSO, and thus its $(G - G_{\rm RP})$ colour index is affected by scattered light from the disc atmosphere. Fig. 7f shows that the new, comoving members are less reddened than the initial members. Neither of them has K_s-band excess, nor *WISE* colour indices characteristic of YSOs. They may represent the discless population of the cluster. We estimated the fraction of disc-bearing stars so that spectroscopically confirmed YSOs with insufficient *Gaia* EDR3 data were included and the comoving stars outside of the cluster were discarded. Thus we obtained $N_{\rm disc}/N_{\rm total} = 0.60$.

L1177. This small globule at $(l,b)=(105°.17,+13°.16)$ contains a single YSO, the FUor-like star 2MASS J21173862+6817340 (Connelley & Reipurth 2018). The lower panel of Fig. 1 suggests a condensation of candidate pre-main-sequence stars, catalogued by Zari et al. (2018), to the north of the globule. We defined a rectangle to encompass the globule and this apparent group of candidate PMS stars. Three confirmed PMS stars of the cloud complex (BD $+68°1118$, [K98c] Em*53, and [K98c] Em*58) are found within the rectangle. The distance and tangential velocity intervals were defined by BD $+68°1118$, [K98c] Em*58 and 28 stars from Zari et al. (2018), and we found 12 further candidate members. [K98c] Em*53 was excluded due to the large errors of its proper motion and RUWE. The most luminous members of the group (Fig. 8e) are the A0-type HD 203533 and the Herbig Ae star BD+68°1118. Figure 8e suggests a mean age of some 5 million years. The star below the 20-Myr isochrone is

the Class I YSO [K98c] Em*58. All these comoving stars are found in a low-extinction region, and according to Fig. 8f, all but two of them are M-type stars without K_s-band excess. The K_s-band-excess stars, 2MASS 21190541+6828465 and 2MASS J21295798+6827007 are new candidate classical T Tauri stars. The colour indices of their *WISE* counterparts confirms its CTTS nature. Figure 8g shows that most of the extinction in this region originates from the distant cloud (the high-velocity sheet in Heiles (1967) and Grenier et al. (1989)). Figure 8a demonstrates that distant star-forming clouds, belonging to the high-velocity complex around 900 pc, are present among the nearby clouds. The molecular cloud [YDM97] CO 23 (Yonekura et al. 1997), marked in Fig. 8a, with its radial velocity of $v_{\rm LSR} = -9.7\,{\rm km\,s^{-1}}$ is part of the distant cloud layer, and the birthplace of the distant classical T Tauri star 2MASS J21225427+6921345 (Kun et al. 2009) ($\varpi = 0.961 \pm 0.110$ mas).

L1217/L1219. L1219 (Barnard 175) has not been observed by *Spitzer*, therefore its YSO population is poorly known. Three T Tauri stars listed in Kun et al. (2009) and the Herbig Fe star BO Cep are projected near the cloud. One of the four YSOs (TYC 4467-324-1) does not fulfil our quality criteria, and another one (BO Cep) differs in the direction of motion from the others. We defined the intervals in Table 2 based on the data of two known T Tauri stars and 23 candidate PMS stars from Zari et al. (2018), and identified 16 further comoving stars clustered around L1219. BD+69°1231, the illuminating star of the bright reflection nebula LBN 110.25+11.38 (Ced 201), and HD 211772, both classified by Zari et al. (2018) as young upper main sequence stars, are members of the group. The average distance of the cluster is 363 ± 2 pc. Figure 9f shows that most of the new candidate members are unreddened M-type stars without K_s-band excess. Six of them have excess emission, characteristic of Class II YSOs, in the *WISE* photometric bands. Figure 9e suggests an age of 1–5 million years.

L1228. L1228 is the northernmost cloud of the Cepheus Flare, and has the largest negative radial velocity ($-7.6\,{\rm km\,s^{-1}}$, Yonekura et al. 1997). The clustering of young stars and candidates projected around L1228 apparently extends beyond the boundaries of the molecular cloud, towards the south-west, where the small, diffuse molecular cloud [YDM97] CO 60 (110.5+19.2) and the CTTS 2MASS J20530638+7450348 can be found. We included this cloud and the stars around 2MASS J20530638+7450348 into the tetragon. Our initial list contains 27 YSOs projected within this area, 17 of which fulfil our astrometric quality criteria. Two of the 17, SSTgbs J2100380+7706598 and [TNK2005] 28 are foreground stars at 291 and 218 pc, respectively. The remaining 15 stars are distributed over a wide distance range between 330 and 404 pc. These stars are probably related to the star-forming history of the region. However, the search for comoving cluster members based on the whole sample resulted in several irrelevant objects, therefore we defined narrower intervals (see Table 2), taking into account only nine stars, projected onto the central ridge of the cloud and 2MASS J20530638+7450348, located at the south-eastern corner of the region. These ten stars are plotted with red squares in Fig. 10. Their average distance of 368 ± 1 pc renders L1228 the most distant cloud of the
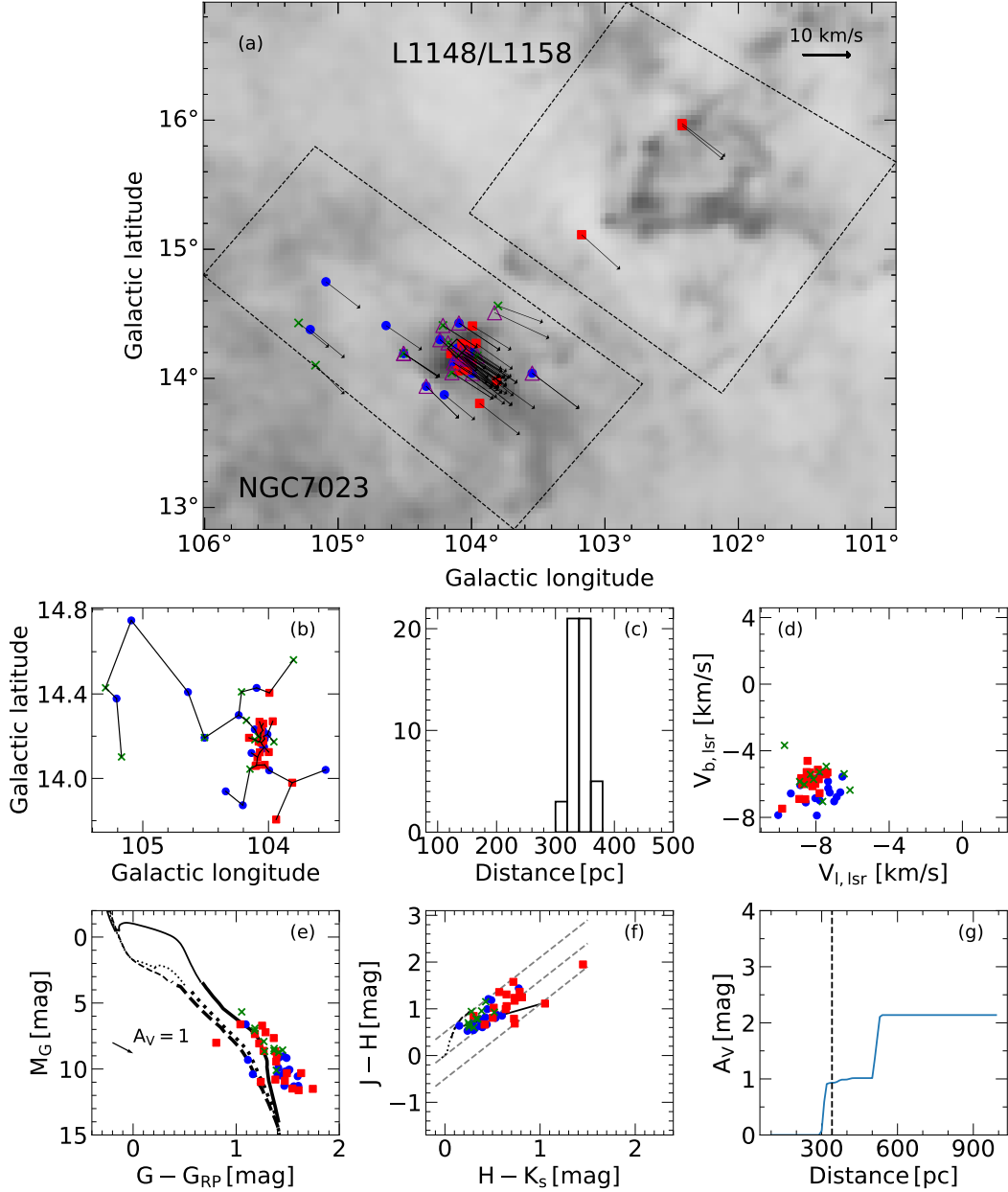
Figure 7. a: Distribution of known YSOs (red squares), YSO candidates (blue circles) and candidate pre-main-sequence stars from Zari et al. (2018) (green crosses) in NGC 7023 and in L1148/L1158, plotted on the *Planck* 857 GHz image. The arrows indicate the tangential velocities of the stars compared to the LSR. Colour codes are same for all other subplots. The black diamond around the filled circle indicates the candidate YSO exhibiting infrared excess in the *WISE* bands. The purple triangles represent candidate cluster members identified by Saha et al. (2020). b: Minimal spanning tree of the stars plotted in panel b. c: Histograms of distances. d: Galactic longitudal vs. latitudal components of tangential velocities compared to the LSR. e: M_G vs. $G - G_{RP}$ colour–magnitude diagram. The thick and thin lines are *CIFIST* and *PARSEC* isochrones, respectively. The solid, dotted, and dashed lines are isochrones of 1, 10, and 20 million years, respectively. f: Colour–Colour-diagram of stars with 2MASS identifiers. g: Visual extinction A_V at the field centre as a function of the distance, obtained from Green et al. (2019). The dashed line shows the mean distance of the stars.

Cepheus flare. Using the distance and velocity intervals defined in Table 2 we identified 36 new candidate members. We found that some stars, mainly in the southern part of the area (Fig. 10a), including GSC 04472-00143 differ in tangential velocities from those projected onto L1228 (L1228N), therefore we divided the stars into two kinematic groups with $v_{b,\mathrm{LSR}} = 0.5\,\mathrm{km\,s^{-1}}$. The spatial distribution of both groups is displayed in Fig. 15, and their average tangential velocities

and distances are shown in Table 4. Figure 15 shows that the groups partly overlap, and Fig. 10c shows that they have the same distance. These stars were probably born in the molecular cloud [YDM97] CO 60, which slightly differs from L1228 in radial velocity. Figure 10e suggests an age of 1 million years. Figure 10f shows that most of the new candidate members are low-mass pre-main-sequence stars, but two stars earlier in spectral type than typical T Tauri type stars are also ap-
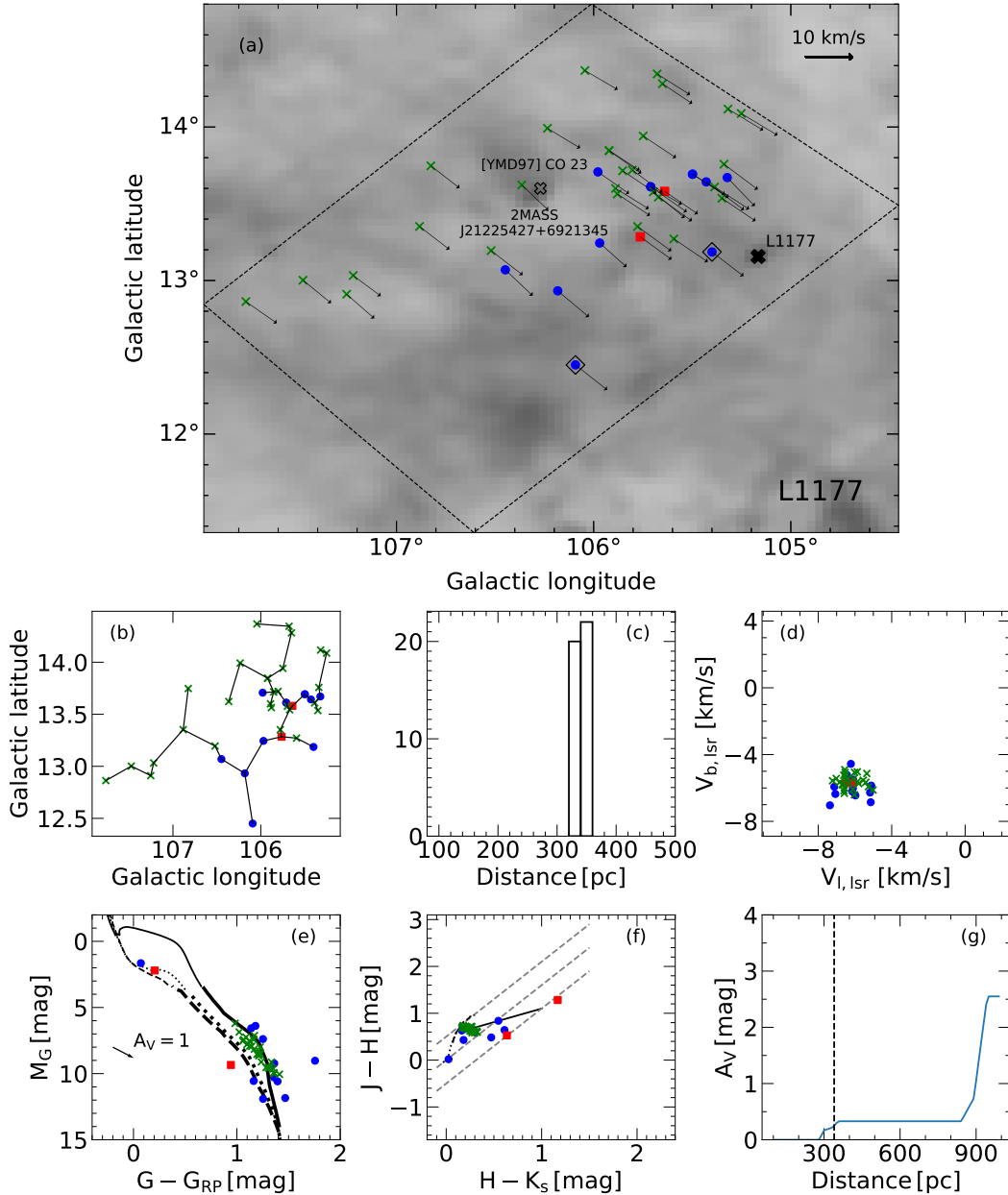
Figure 8. Same as Figure 7 for L1177.

parent in these figures. One of them is BD+76°825, associated with the reflection nebula GN 21.01.8, and the other is TYC 4590-843-1. Both stars are situated near the cloud centre and are coincide in proper motion with the known YSOs of the cloud. Six candidate group members, located outside of the area observed by *Spitzer*, have infrared excesses characteristic of Class II YSOs in the *WISE* bands. The fraction of disc-bearing stars is about 52.6% for the northern group, and 22% for the southern group, suggesting the more evolved nature of the latter.

L1235. L1235 has not been observed by *Spitzer*, therefore its YSO population is less well mapped. The known young stellar population associated with L1235 consists of three classical T Tauri stars, listed in Kun et al. (2009), and the Herbig Ae

Table 4. Average distances and tangential velocities (compared to the LSR) of the two kinematic subgroups of L1228 and HD 190833 group.

Group	d_{avg} (pc)	$v_{l,lsr,avg}$ (km s^{-1})	$v_{b,lsr,avg}$ (km s^{-1})
L1228 North	366.93 ± 6.47	-3.66 ± 0.72	1.55 ± 0.48
L1228 South	367.98 ± 6.92	-4.71 ± 1.09	-0.38 ± 0.51
HD 190833	184.65 ± 8.01	-1.84 ± 0.33	-0.05 ± 0.39
	177.51 ± 6.97	-2.42 ± 0.55	2.32 ± 0.32

star SV Cep. More recent star formation in the core of the cloud is indicated by the submillimeter sources observed by the SCUBA instrument on the JCMT (Di Francesco et al.
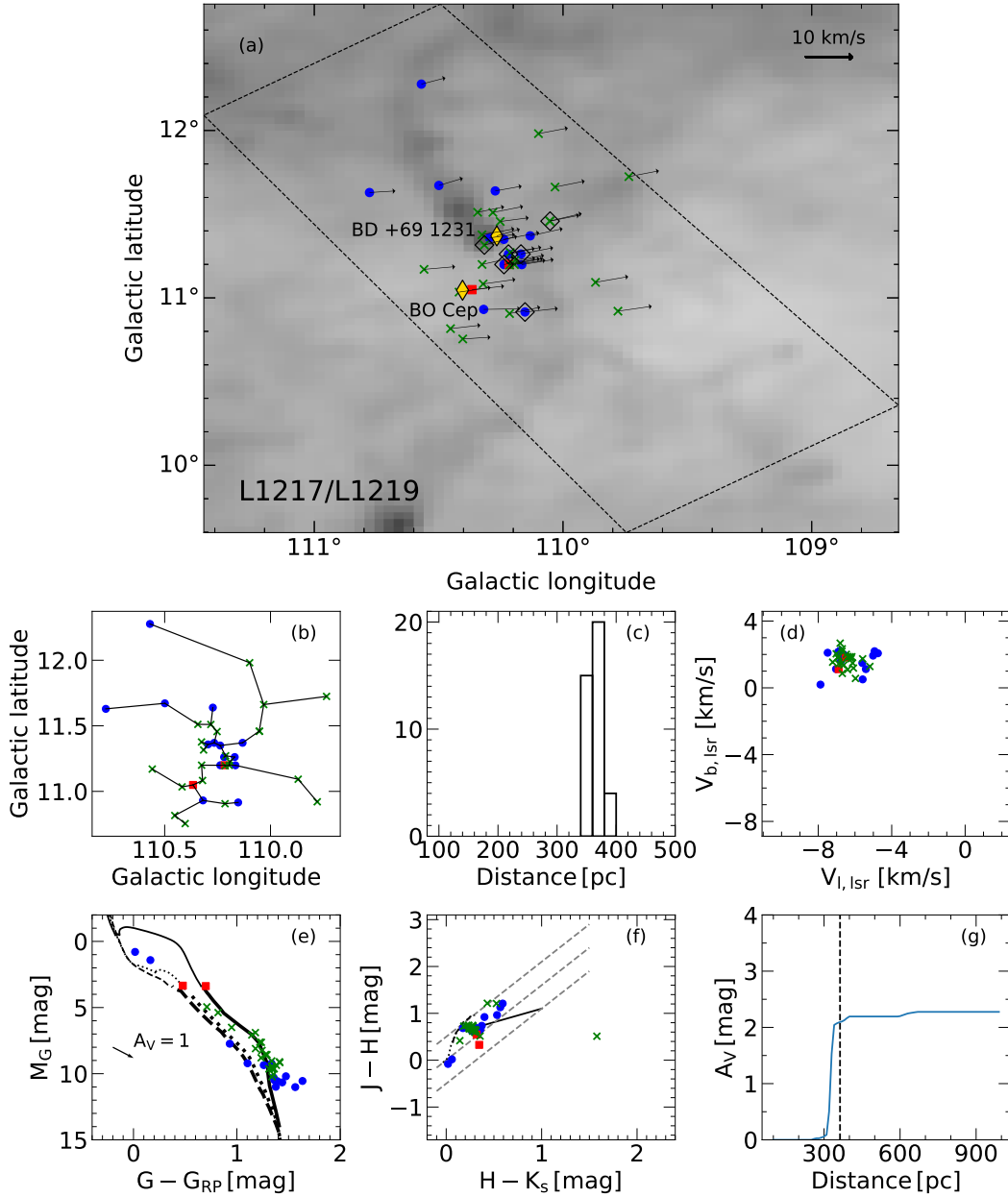
Figure 9. Same as Fig. 7 for L1217/1219.

2008). Our search revealed 68 candidate members, coinciding in parallax and proper motion with the T Tauri stars listed in Kun et al. (2009), and also with the B8-type stars BD +72°1018 and HD 210806, illuminating reflection nebulae embedded in L1235. Thirty-two of the 68 candidate members are included in Zari et al. (2018), and 12 of them have Class II-like infrared excess in the *WISE* bands, including the *Gaia* Photometric Science Alert source Gaia 19bny. Figure 11e suggests ages 1–5 million years.

L1251. Our initial list of YSOs contains 31 stars associated with L1251. Fourteen of them fulfil our astrometric criteria. These stars are plotted with red squares in Fig. 12. We identified 54 stars coinciding in distance and velocity with these stars, and 26 of them is included in the catalogue of Zari

et al. (2018). Figure 12a shows that most of the new candidate members are located outside of the cloud. Figure 12e suggests an age of 1–5 million years, and 12f shows that most of the new candidate members are M-type pre-main-sequence stars. Six of them exhibit infrared excess, characteristic of Class II YSOs in the *WISE* wavelength region, and two of them bear transitional discs. The highest mass star of the group is the A0 type star HD 216367, classified as young upper-main-sequence star by Zari et al. (2018). The fraction of disc-bearing stars is apparently higher inside the cloud (28/41) than outside (9/37), indicating the more evolved nature of the off-cloud population, but these numbers are affected by the different sensitivities of *Spitzer* and *WISE*.
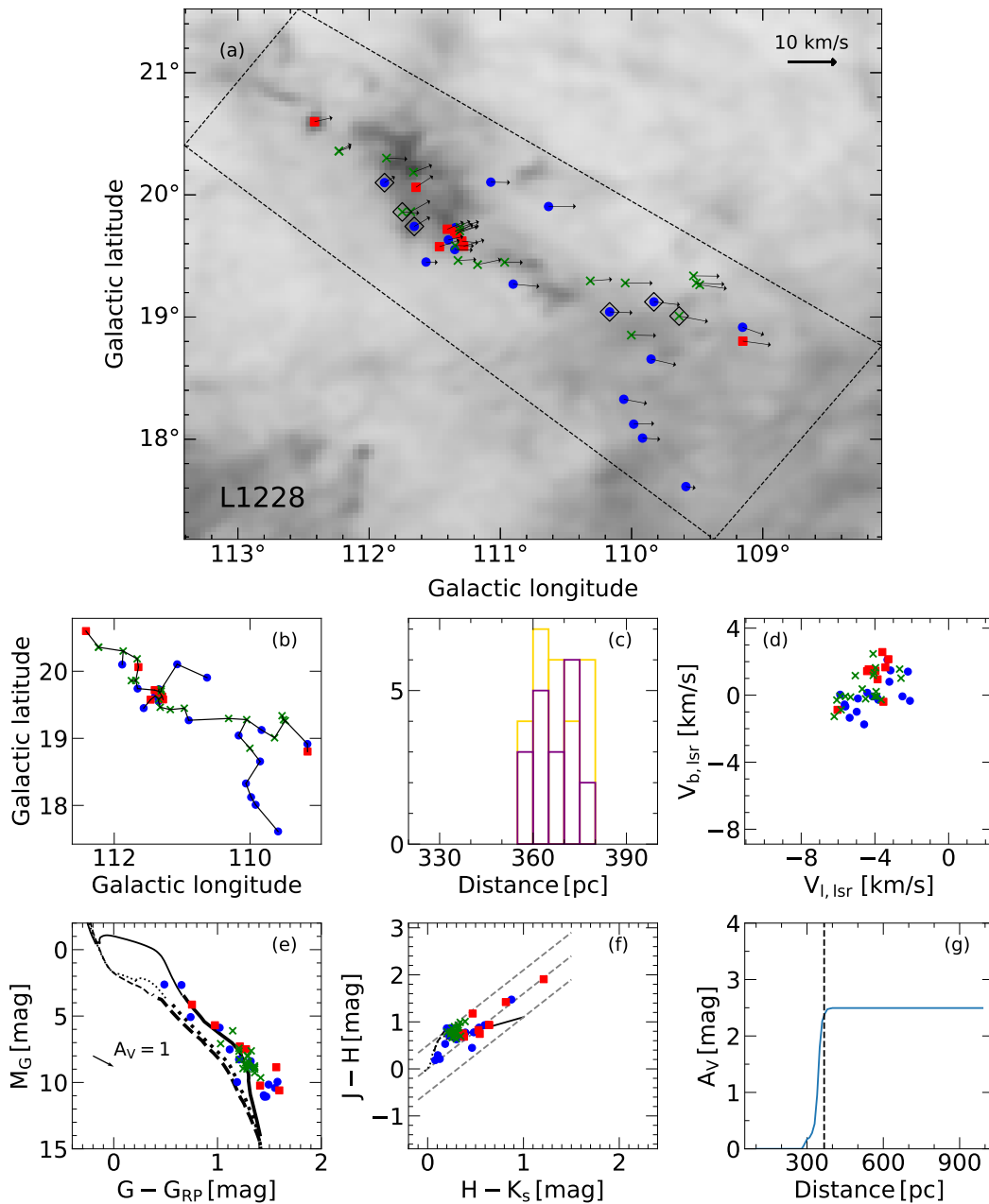
Figure 10. Same as Fig. 7 for L1228. The purple and gold colors on panel *c* show the distances of northern and southern subgroups, respectively.

4.1 Pre-main-sequence stars nearer than 200 pc

L1262 (CB 244). This small globule contains the low-luminosity embedded protostar IRAS 23238+7401 (Pollanen & Feldman 1995). Two optically visible YSOs, AS 507 and [K98c] Em*137, projected on this cloud, have distances of 189 and 197 pc, respectively, thus we adopt the distance 194 pc for the cloud. AS 507 has a companion at 9.3 arcsec separation (Kun et al. 2009). The *Gaia* data revealed that both stars have similar distances and tangential velocities. L1262 is the only molecular cloud projected within the volume of the Cepheus Association. However, only AS 507 fulfils the kinematic membership criteria.

Cepheus Association. We identified 37 new candidate members of the association within the $11° \times 10°$ area indicated in Fig. 1 (see Sect. 3.2). These stars have a mean distance ($\pm$ standard error of the mean) of 161 ± 2 pc. Figures 13e and 13f show that the new candidate members represent the M-type population of the association. The two apparent outliers in Fig. 13e correspond to the two stars located near the low-latitude boundary of the region, AS 507 and 2MASS J23222636+7414115. According to Fig. 4 their space velocities are consistent with those of the other association members. The divergent v_b positions result from their different Galactic latitudes. Fig. 13e suggests an age of some 20 million years. These stars are older than the stars of the
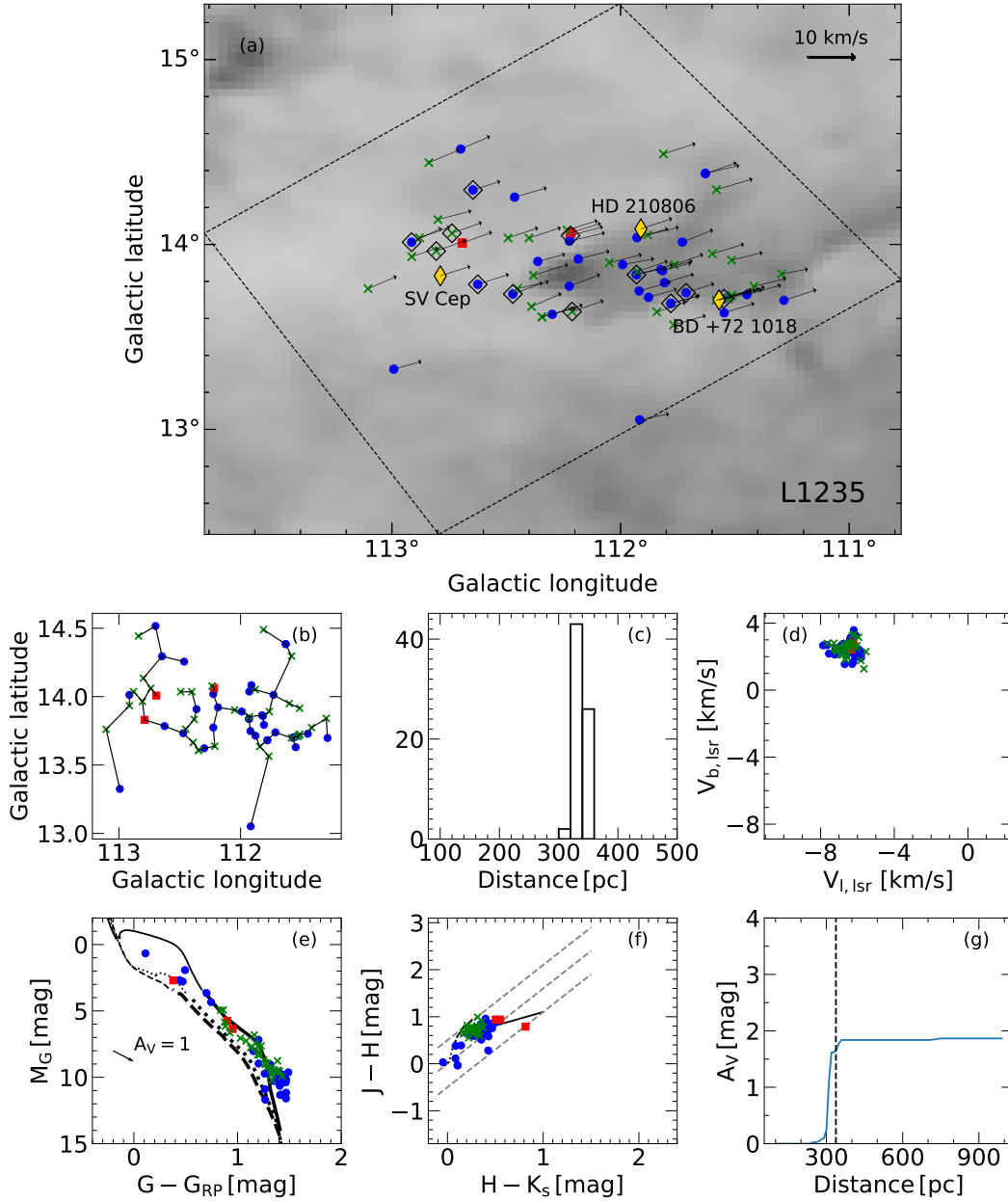
Figure 11. Same as Fig. 7 for L1235.

HD 190833 Group. We identified 46 candidate members of the group. Similarly to the Cepheus Association, these sources are older and are not associated with cloud. Four of them show infrared excesses, characteristic of Class II YSOs in the *WISE* wavelength region. The two subgroups, revealed by the *W* distribution in Fig. 4, are apparent also in Fig. 14a and Fig. 14d. Their mean distances and velocities are listed in Table 4. Figure 14e shows that both subgroups are coeval, about 10–12 Myr old. The presence of some 10 % disc-bearing stars is noteworthy at this age.

molecular clouds, and their parental cloud had possibly dispersed.

4.2 Young stars beyond 500 pc

Our search for new candidate members of the Cepheus flare clouds was not extended beyond 500 pc. Table A1, however, shows that a few young stars, projected onto the molecular clouds, are background stars around 900–1000 pc. Massive H I and CO clouds, associated with the Local Arm of the Galaxy are present in the high-latitude regions of Cepheus (Heiles 1967; Grenier et al. 1989, respectively) in this distance interval. The YSO candidate *Spitzer* sources around 1 kpc, projected onto the L1148/L1177 complex (see the black symbols in the lower panel of Fig. 1) may be associated with this cloud complex.

Another distant YSO, apparently not associated with known molecular cloud is the southern component of the visual double [K98c] EM*119. Its components,
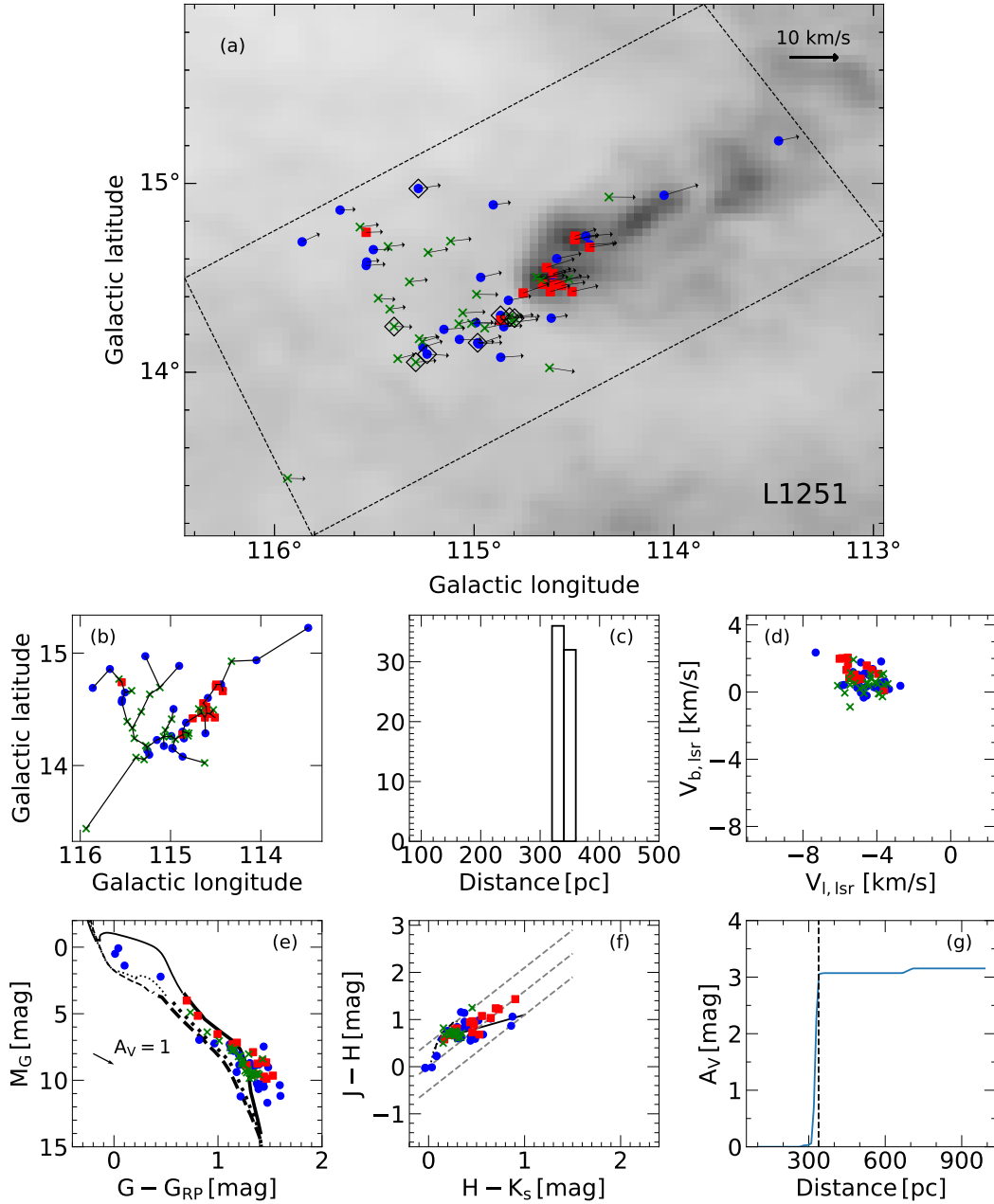
Figure 12. Same as Fig. 7 for L1251.

[KBK2009b] Em* 119 S and [KBK2009b] Em* 119 N are separated by 4 arcsec, and both stars exhibit classical T Tauri spectra (Kun et al. 2009). The northern component has a distance of 327^{+34}_{-26} pc, however the large RUWE value renders its *Gaia* EDR3 data uncertain. The distance of the southern component is 907^{+29}_{-23} pc, with RUWE = 1.1. The 3D extinction map of Green et al. (2019) at the position of this star shows that the low extinction of $E(g-r) = 0.14$ mag rises to 0.68 mag around 900 pc. A similar visual double is [TNK2005] 37 is found in the same part of the studied region. The brighter component [TNK2005] 37 c1 is a weak-line T Tauri star (Tachihara et al. 2005) at 974^{+8}_{-9} pc.

5 OVERALL VIEW OF THE CEPHEUS FLARE REGION

Table 5 shows that the YSOs in the Cepheus flare are located between 330 and 370 pc. The star-forming clouds in the $12° \lesssim b \lesssim 16°$ Galactic latitude interval, L1147/L1158, L1172/L1174, L1177, L1235, and L1251, are between 330 and 341 pc. The clouds outside this latitude interval, L1217/L1219 and L1228 are 20–30 pc farther. These results indicate a line-of-sight dimension of the cloud complex significantly smaller than its $\sim 90 \times 60$ pc size, perpendicular to the line of sight. This is in accordance with the results of Heiles (1967), who found similar, sheet-like structure in the H I counterpart of the cloud complex.

Figure 5 suggests that the large velocity dispersion reported by Dzib et al. (2018) results from the kinematic dif-
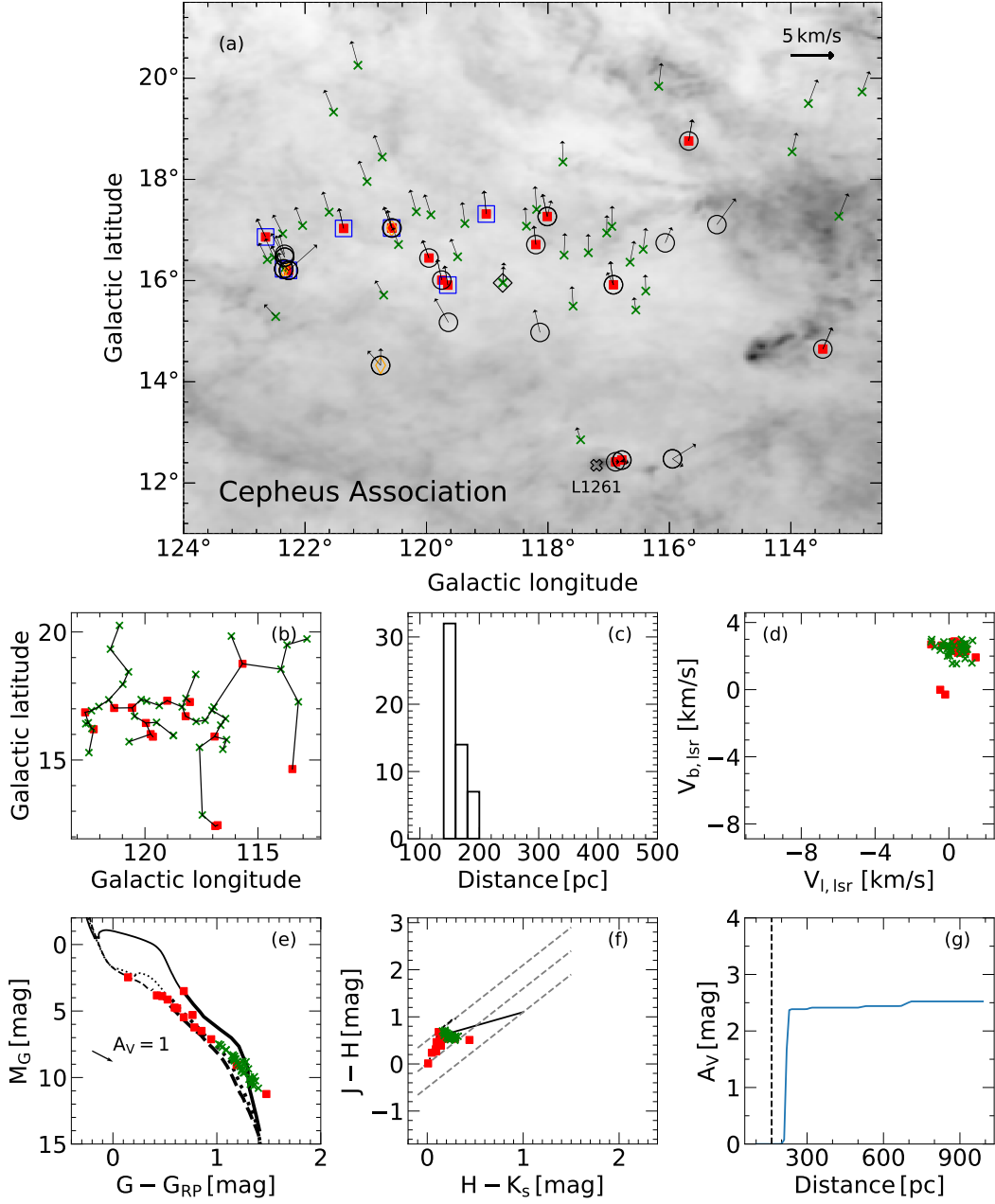
Figure 13. Same as Fig. 7 for the Cepheus association. The orange diamonds, blue squares and black empty circles are showing sources from Guillout et al. (2010), Faherty et al. (2018) and Cepheus association members from Klutsch et al. (2020), respectively.

ferences between the clouds. The substructures of the region also differ from each other in the radial velocity of the molecular gas (Yonekura et al. 1997). Radial velocities are available only for a few stars, and their uncertainties hinder any conclusion. To get an insight into the internal motions of the complex we assume that the average velocities of the YSOs and their natal clouds are similar and combine the tangential velocities of the stars with radial velocities of the clouds. The symbol colours in Fig. 16 indicate three distinct radial velocity intervals of the molecular clouds. Arrows indicate the mean tangential velocities of the young stellar groups associated with the clouds compared to the average of the whole system. Symbol sizes indicate distances.

The tangential and radial velocities reveal three kinematic groups. The clouds in the western part of the complex, L1148/L1158, L1172/L1174, and L1177 form a spatially and kinematically coherent structure. Their star-forming histories are probably connected. An age gradient of the comoving stars can be seen in the L1148/L1177 sytem. Whereas no discless star and several embedded YSOs, not detected by *Gaia*, are found in the region of L1147/L1148, 90 % of the comoving stars around L1177 are discless low-mass stars. This large structure overlaps in projection with the slightly more distant cluster *Theia 5* identified by Kounkel & Covey (2019).

The second, apparently kinematically coherent subsystem

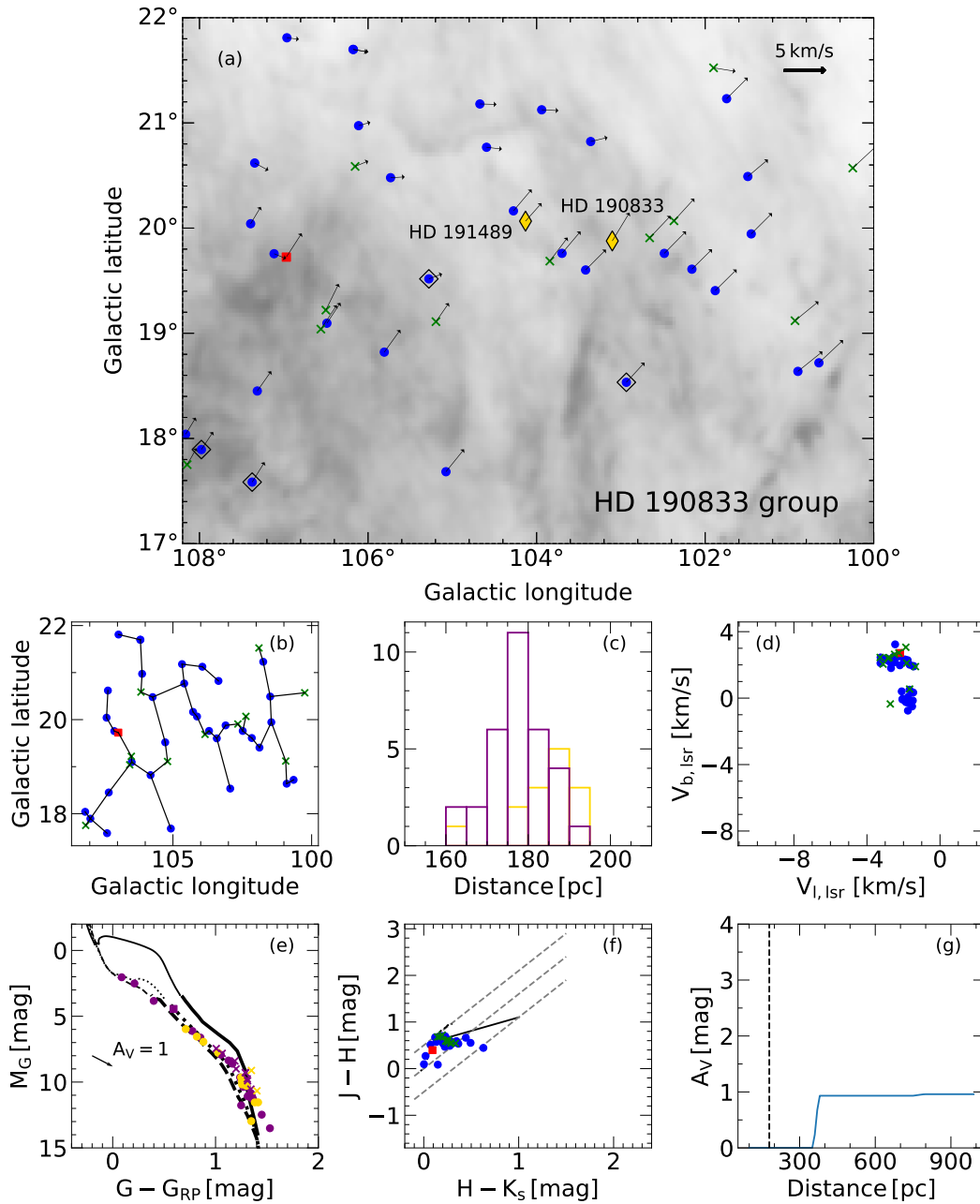**Figure 14.** Same as Fig. 7 for the HD 190833 group. The purple and gold colours on panel *c* and *e* show the distance histograms and the colour-magnitude diagrams of the two kinematic subgroups, respectively.

consists of L1219, L1235, and L1251. The tangential velocities of the comoving stars in L1219 and L1235 are similar, but L1219 is some 25 pc farther than L1235. Star formation in L1219 was probably influenced by the supershell G113+10 from the southern direction (Bally & Reipurth 2001; Kiss, Moór & Tóth 2004). The morphology of the region suggests that the star formation in L1235 might have been affected by the same supershell. L1251 is close to L1235 and both clouds have similar radial velocities, but their star-forming histories appear quite different. The cometary shape of L1251 is indicative of star formation triggered by shock waves from the CFS (Tóth & Walmsley 1996; Olano et al. 2006). The conspicuous cluster of stars, located on the head side of the

cloud, and the apparent age gradient of YSOs observed across L1251 support this scenario.

The third kinematic group of the region is L1228 at the highest Galactic latitude, at the distance of 368 pc, and with the radial velocity of -7.6 kms. Several arguments suggest that star formation in L1228 was also affected by the Cepheus Flare Shell (Kirk et al. 2009). L1228 is some 30 pc farther than L1251, thus we can have a glimpse into the three-dimensional structure of the CFS. Whereas in the case of L1251 the shock from the supershell propagates in the east–west direction, largely perpendicular to the line of sight, L1228 and the adjacent [YDM97] CO 60 are located towards the far side of the shell, where the expansion has a line-of-sight cmponent. The

Table 5. Average parallaxes, distances (from Bailer-Jones et al. (2021)), and tangential velocities with the standard errors of the mean, and standard deviations (σ) for different substructures.

Cloud	N*	N_{cand}	ϖ_{avg} (mas)	σ_ϖ	d_{avg} (pc)	σ_d	$v_{l,lsr,avg}$ (km s^{-1})	σ_{v_l}	$v_{b,lsr,avg}$	σ_{v_b}	L_{avg} (MST) (pc)
NGC 7023	50	31	2.906 ± 0.016	0.112	341 ± 2	13	-8.07 ± 0.12	0.84	-6.00 ± 0.11	0.81	0.540
L1148/L1158	3	0	2.978 ± 0.011	0.024	330 ± 1	3	-8.73 ± 0.24	0.51	-7.48 ± 0.08	0.17	3.261
L1177	42	40	2.911 ± 0.010	0.063	340 ± 1	8	-6.22 ± 0.09	0.60	-5.74 ± 0.08	0.51	1.087
L1217/L1219	39	37	2.719 ± 0.016	0.099	363 ± 2	13	-6.39 ± 0.11	0.70	1.63 ± 0.09	0.54	0.737
L1228	46	36	2.684 ± 0.007	0.050	368 ± 1	7	-4.27 ± 0.16	1.08	0.42 ± 0.16	1.08	1.176
L1235	71	68	2.930 ± 0.008	0.069	338 ± 1	8	-6.51 ± 0.06	0.50	2.45 ± 0.05	0.43	0.597
L1251	68	54	2.915 ± 0.008	0.063	339 ± 1	8	-4.66 ± 0.10	0.83	0.70 ± 0.08	0.65	0.619
Cepheus Ass.	53	37	6.214 ± 0.063	0.463	161 ± 2	13	0.29 ± 0.08	0.58	2.34 ± 0.08	0.61	1.883
HD 190833 g.	46	45	5.543 ± 0.036	0.250	180 ± 1	8	-2.24 ± 0.08	0.56	1.60 ± 0.17	1.15	1.690

*Total number of group members with reliable astrometric data in *Gaia* EDR3.
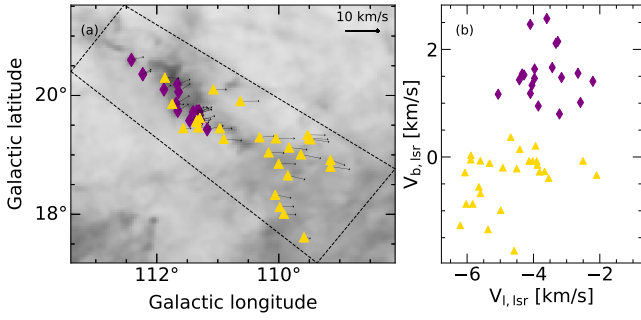

Figure 15. Surface distribution and tangential velocities of two kinematic subgroups of L1228.
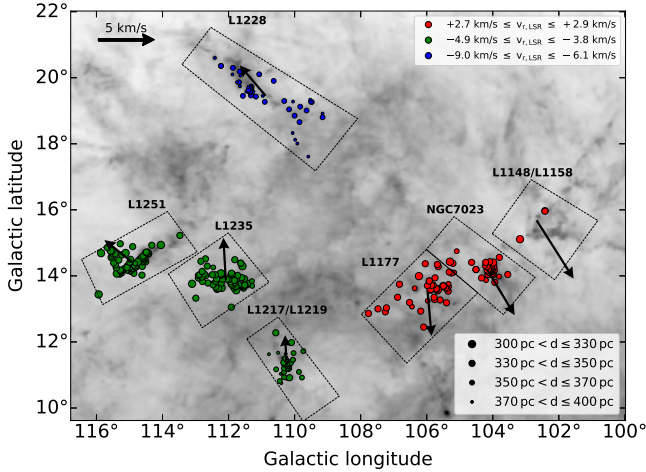

Figure 16. Average tangential velocities of the stars associated with molecular clouds compared to the average of all known YSOs between 300 and 400 pc. The colours indicate the radial velocities of the parental cloud (Yonekura et al. 1997), with respect to the LSR.

wide range of distances of the YSOs projected around L1228 in Table A1 supports the scenario that star formation propagates largely along the line of sight, thus stars of different ages may be located at different distances.

The MSTs show that small, compact clusters are associated with NGC 7023, L1219, L1228, L1235, and L1251, whereas loose aggregates of a few stars are associated with the L1148/L1158 complex and L1177. The comoving groups do not fill the defined tetragons, confirming that they are real clusters associated with the central molecular clouds. We examined the cumulative distribution of the MST branch lengths, and determined the average length following the method described by Gutermuth et al. (2009). The results are shown in the last column of Table 5. The average separations of the group members are 5–10 times larger than those of the young clusters observed by *Spitzer*, reflecting the more evolved nature of our groups.

The colour–magnitude diagrams suggest ages of 1–5 million years. Spectroscopic follow-up observations are essential for precise age determination. Whereas 85 per cent of the stars in our initial list are disc-bearing YSOs, 87 % of the new candidate group members represent the discless population of the clouds.

The Cepheus flare star-forming region is comparable in size and stellar content to the Taurus and Lupus clouds, however differs from them in structure and thus probably in star-forming history. The most striking difference is that whereas the Taurus clouds closely cluster around the central ridge of the cloud complex, and only a few smaller clouds are found in the outskirts of the region, star formation in the Cepheus flare occurs at the edges of the cloud complex. No young stars can be found in the central regions. Furthermore the depth of the Taurus complex is comparable with its projected size (Galli et al. 2019), whereas the Cepheus flare has a sheet-like shape. Unlike the YSOs of the Lupus clouds (Galli et al. 2020), stars in the Cepheus clouds form several kinematic subsystems. The overall picture of the region in view of the *Gaia* data confirms the scenario that the strucure of the cloud complex and star formation was probably shaped by shocks from energetic stellar winds and multiple supernovae.

The distance of 160–180 pc of the nearby groups of pre-main-sequence stars suggests their association with the wall of the Local Bubble (e.g Lallement et al. 2003). The boundaries of the Local Bubble are defined by interstellar clouds, showing up as extinction of the starlight or interstellar absorption lines in stellar spectra. Figure 13e suggests a small amount of reddening of the candidate pre-main-sequence association members. A colour excess $E(BP - RP) =$

0.205 mag, listed for HD 190833 in the *Gaia* DR2, also indicates a thin cloud toward the line of sight of this star. The mean ages of the groups are compatible with the age of the Local Bubble (14.6 Myr, Breitschwerdt & de Avillez 2006).

6 CONCLUSIONS

We studied the distribution and kinematics of the stars in the region $100° < l < 125°$, $8° < b < 22°$, based on the *Gaia* EDR3 data. The area studied contains the molecular cloud complex of the Cepheus flare and the adjacent cloud-free region. We identified *Gaia* EDR3 counterparts of 176 stars, classified as YSOs in the literature.

Based on the distances and tangential velocities of the known YSOs we found 266 additional candidate members of the molecular clouds. The colour–magnitude diagrams of the YSO groups suggest ages of 1–5 million years. 85 % of the stars in the initial list are disc-bearing YSOs, and 87 % of the new candidate group members represent the discless population of the clouds.

The star-forming clouds in the $12° \lessapprox b \lessapprox 16°$ Galactic latitude interval, L1147/L1158, L1172/L1174, L1177, L1235, and L1251, have distances between 330 and 341 pc. The clouds outside this latitude interval, L1217/L1219 and L1228 are 20–30 pc farther. These distances suggest that the line-of-sight dimension of the cloud complex is significantly smaller than its $\sim 90 \times 60$ pc size, perpendicular to the line of sight.

We found that the clouds of the Cepheus flare form three major kinematic subsystems: (i) L1147/L1148, L1172/L1174, and L1177, (ii) L1219, L1235, and L1251, (iii) L1228.

We identified two kinematically distinct subgroups of candidate PMS stars around L1228. The southern subgroup is associated with a small and diffuse molecular cloud [YDM97] CO 60.

The 71 comoving stars associated with L1235, including the B8 type stars HD 210806 and BD +72°1018 and the Herbig Ae star SV Cep suggest the richest cluster of the Cepheus flare.

We found a cluster of comoving stars, located on the head side of the cometary-shaped L1251. Comparison of the disc fractions of the off-cloud and on-cloud groups suggests an age gradient which fits into the scenario of triggered star formation.

The *Gaia* parallaxes reveal a foreground population of pre-main-sequence stars, probably associated with the boundaries of the Local Bubble, and a few background stars, probably associated with the clouds of the Galactic Local Arm.

We identified 37 new candidate members of the nearby Cepheus Association, at a distance of 161 pc.

A new moving group of 46 candidate pre-main-sequence stars were identified around HD 190833, at a mean distance of 180±1 pc.

DATA AVAILABILITY

The data underlying this article are available at Vizier at https://vizier.u-strasbg.fr/viz-bin/VizieR. The datasets were derived from sources in the public domain of *Gaia* at https://gea.esac.esa.int/archive/.

REFERENCES

Ábrahám P., Balázs L. G., Kun M., 2000, A&A, 354, 645
Astropy Collaboration et al., 2013, A&A, 558, A33
Astropy Collaboration et al., 2018, AJ, 156, 123
Bailer-Jones C. A. L., Rybizki J., Fouesneau M., Demleitner M., Andrae R., 2021, AJ, 161, 147
Bally J., Reipurth B., 2001, ApJ, 552, L159
Baraffe I., Homeier D., Allard F., Chabrier G., 2015, A&A, 577, A42
Berkhuijsen E. M., 1973, A&A, 24, 143
Breitschwerdt D., de Avillez M. A., 2006, A&A, 452, L1
Bressan A., Marigo P., Girardi L., Salasnich B., Dal Cero C., Rubele S., Nanni A., 2012, MNRAS, 427, 127
Clemens D. P., Barvainis R., 1988, ApJS, 68, 257
Connelley M. S., Reipurth B., 2018, ApJ, 861, 145
Connelley M. S., Reipurth B., Tokunaga A. T., 2008, AJ, 135, 2496
Damiani F., Prisinzano L., Pillitteri I., Micela G., Sciortino S., 2019, A&A, 623, A112
Di Francesco J., Johnstone D., Kirk H., MacKenzie T., Ledwosinska E., 2008, ApJS, 175, 277
Dzib S. A., Loinard L., Ortiz-León G. N., Rodríguez L. F., Galli P. A. B., 2018, ApJ, 867, 151
Faherty J. K., Bochanski J. J., Gagné J., Nelson O., Coker K., Smithka I., Desir D., Vasquez C., 2018, ApJ, 863, 91
Froebrich D., 2005, ApJS, 156, 169
Gaia Collaboration et al., 2016, A&A, 595, A1
Gaia Collaboration et al., 2018, A&A, 616, A1
Gaia Collaboration et al., 2021, A&A, 649, A1
Galli P. A. B., et al., 2019, A&A, 630, A137
Galli P. A. B., et al., 2020, A&A, 643, A148
Ginsburg A., et al., 2019, AJ, 157, 98
Green G., 2018, The Journal of Open Source Software, 3, 695
Green G. M., Schlafly E., Zucker C., Speagle J. S., Finkbeiner D., 2019, ApJ, 887, 93
Greene T. P., Wilking B. A., Andre P., Young E. T., Lada C. J., 1994, ApJ, 434, 614
Grenier I. A., Lebrun F., Arnaud M., Dame T. M., Thaddeus P., 1989, ApJ, 347, 231
Guillout P., Frasca A., Klutsch A., Marilli E., Montes D., 2010, A&A, 520, A94
Gutermuth R. A., Megeath S. T., Myers P. C., Allen L. E., Pipher J. L., Fazio G. G., 2009, ApJS, 184, 18

_____

[1] http://www.astropy.org

Heiles C., 1967, ApJS, 15, 97

Hubble E., 1934, ApJ, 79, 8

Hunter J. D., 2007, Computing in Science & Engineering, 9, 90

Kirk J. M., et al., 2009, ApJS, 185, 198

Kiss C., Moór A., Tóth L. V., 2004, A&A, 418, 131

Klutsch A., Frasca A., Guillout P., Montes D., Pineau F. X., Grosso N., Stelzer B., 2020, A&A, 637, A43

Koenig X. P., Leisawitz D. T., 2014, ApJ, 791, 131

Kounkel M., Covey K., 2019, AJ, 158, 122

Kun M., 1998, ApJS, 115, 59

Kun M., Balázs L. G., Tóth I., 1987, Ap&SS, 134, 211

Kun M., Kiss Z. T., Balog Z., 2008, in Reipurth, B. ed., , Handbook of Star Forming Regions, Volume I. ASP: San Francisco, p. 136

Kun M., Balog Z., Kenyon S. J., Mamajek E. E., Gutermuth R. A., 2009, ApJS, 185, 451

Lallement R., Welsh B. Y., Vergely J. L., Crifo F., Sfeir D., 2003, A&A, 411, 447

Lindegren L., 2018, Re-normalising the astrometric chi-square in Gaia DR2, GAIA-C3-TN-LU-LL-124

McKinney W., 2010, in van der Walt S., Millman J., eds, Proceedings of the 9th Python in Science Conference. pp 51 – 56

Olano C. A., Meschin P. I., Niemela V. S., 2006, MNRAS, 369, 867

Page L., et al., 2007, ApJS, 170, 335

Pollanen M. D., Feldman P. A., 1995, PASP, 107, 617

Reid M. J., et al., 2014, ApJ, 783, 130

Saha P., Gopinathan M., Kamath U., Lee C. W., Puravankara M., Mathew B., Sharma E., 2020, MNRAS, 494, 5851

Schönrich R., Binney J., Dehnen W., 2010, MNRAS, 403, 1829

Skrutskie M. F., et al., 2006, AJ, 131, 1163

Tachihara K., Neuhäuser R., Kun M., Fukui Y., 2005, A&A, 437, 919

Taylor M. B., 2005, in Shopbell P., Britton M., Ebert R., eds, Astronomical Society of the Pacific Conference Series Vol. 347, Astronomical Data Analysis Software and Systems XIV. p. 29

Tóth L. V., Walmsley C. M., 1996, A&A, 311, 981

VanderPlas J., 2016, Journal of Open Source Software, 1, 12

Wright E. L., et al., 2010, AJ, 140, 1868

Yonekura Y., Dobashi K., Mizuno A., Ogawa H., Fukui Y., 1997, ApJS, 110, 21

Young C. H., et al., 2009, ApJ, 702, 340

Zari E., Hashemi H., Brown A. G. A., Jardine K., de Zeeuw P. T., 2018, A&A, 620, A172

Zucker C., Speagle J. S., Schlafly E. F., Green G. M., Finkbeiner D. P., Goodman A., Alves J., 2020, A&A, 633, A51

This paper has been typeset from a TEX/LATEX file prepared by the author.

APPENDIX A: LISTS OF YOUNG STELLAR OBJECTS OF THE CEPHEUS FLARE PUBLISHED IN *Gaia* EDR3

Table A1. Sample of YSOs contained in our initial list. The full table is available as supplementary material.

Name	Gaia EDR3 ID	2MASS designation	RA (J2016) (deg)	DEC (J2016) (deg)	$\mu_\alpha^\star$ (mas yr^{-1})	μ_δ (mas yr^{-1})	ϖ (mas)	Distance* (pc)	RUWE
2MASS J00003379+7940362	564638120384153472	00003379+7940362	0.1414	79.6767	22.753	0.122	6.456 ± 0.025	$153.9^{+0.5}_{-0.5}$	0.993
BD+78 853	564638150446547200	00004121+7940398	0.1723	79.6778	23.013	0.789	6.463 ± 0.014	$154.3^{+0.3}_{-0.4}$	0.917
2MASS J00134052+7702104	540216042986714368	00134052+7702104	3.4182	77.0361	20.177	−1.652	5.887 ± 0.029	$169.1^{+0.8}_{-0.8}$	1.697
TYC 4496-780-1	540216042984524800	00134052+7702104	3.4195	77.0364	21.892	−1.608	5.883 ± 0.012	$169.5^{+0.3}_{-0.3}$	0.970
TYC4500-616-1	564977079203963648	00172828+7947580	4.3684	79.7994	22.244	−1.105	6.330 ± 0.019	$157.5^{+0.5}_{-0.4}$	1.547
2MASS J00380313+7903194	564698451789359104	00380313+7903194	9.5137	79.0554	24.969	−4.077	6.726 ± 0.016	$148.3^{+0.4}_{-0.4}$	1.291
[TNK2005] 4c1	564698451788613376	00380610+7903206	9.5260	79.0557	18.500	−2.339	6.817 ± 0.048	$146.5^{+1.3}_{-1.0}$	4.070
2MASS J00390355+7919191	564707973733132032	00390355+7919191	9.7654	79.3220	23.633	−3.009	6.583 ± 0.023	$151.6^{+0.6}_{-0.5}$	1.739
2MASS J00390430+7922350	564802050695978752	00390430+7922350	9.7685	79.3764	23.771	−3.519	6.751 ± 0.066	$147.0^{+1.4}_{-1.3}$	1.088
[TNK2005] 5c1	564707973733132800	00390619+7919096	9.7764	79.3193	24.209	−2.477	6.584 ± 0.118	$152.2^{+2.2}_{-2.5}$	8.809
2MASS J00393878+7905160	564695879105289344	00393878+7905160	9.9122	79.0878	24.510	−2.834	6.667 ± 0.036	$149.0^{+0.8}_{-0.9}$	1.008

*Distance from Bailer-Jones et al. (2021)

Table A2. Column description of the table containing the YSOs and candidates. The list is available as supplementary material. The stars of the close groups and of the clouds are separated into two tables.

Column	Description
cloud	Group identifier
Name	Star-identifier
designation	Gaia EDR3 identifier
TMASS	2MASS identifier
ra	RA at J2016
dec	DEC at J2016
l	Galactic longitude
b	Galactic latitude
r_med_geo	Distance from Bailer-Jones et al. (2021)
r_lo_geo	16th percentile of distance posterior from Bailer-Jones et al. (2021)
r_hi_geo	84th percentile of distance posterior from Bailer-Jones et al. (2021)
parallax	Parallax
parallax_error	Error of the parallax
pmra	Proper motion in right ascension
pmra_error	Error of the proper motion in right ascension
pmdec	Proper motion in declination
pmdec_error	Error of the proper motion in declination
tang_vel_l	Tangential velocity in galactic longitude
tang_vel_b	Tangential velocity in galactic latitude
phot_g_mean_mag	Magnitude in G band
phot_bp_mean_mag	Magnitude in G_{BP} band
phot_rp_mean_mag	Magnitude in G_{RP} band
Jmag	Magnitude in 2MASS J band
Hmag	Magnitude in 2MASS H band
Kmag	Magnitude in 2MASS Ks band
ruwe	Renormalized unit-weight error

Table A3. Sample of the candidate disc-bearing YSOs classified by WISE/2MASS data. The full table is available as supplementary material.

Name	allwise_id	type
2MASS J20144588+6942055	J201445.91+694205.5	Class II
2MASS J20171018+7207013	J201710.24+720701.5	Class II
2MASS J20525705+7245414	J205257.07+724541.5	Class II
2MASS J20541245+7324249	J205412.49+732424.8	Class II